ANALYSIS OF THE SPATIAL CORRELATION MEASUREMENTS FOR THE MULTIPLE INPUT MULTIPLE OUTPUT (MIMO) CHANNEL USING ANECHOIC CHAMBER MEASUREMENT METHODOLOGIES TO EVALUATE OVER-THE-AIR (OTA) TESTING TECHNIQUES

by

DIGVIJAY ARJUNRAO JADHAV

Presented to the Faculty of the Graduate School of

The University of Texas at Arlington in Partial Fulfillment

of the Requirements

for the Degree of

MASTER OF SCIENCE IN ELECTRICAL ENGINEERING

THE UNIVERSITY OF TEXAS AT ARLINGTON

December 2009

ACKNOWLEDGEMENTS

I would like to express my deepest appreciation to my committee chair, Dr.Jonathan Bredow, who believed in me and gave me this wonderful opportunity to work with him in the Wave Scattering Research Centre at The University of Texas at Arlington. On personal note I would like to mention that he is a teacher who motivated me to learn by principle some of the important aspects of the RF Engineering and Microwave Systems Engineering. He always showed concern to my view points and boosted my confidence by guiding me throughout my Masters at UTA. I always admired his dedication and persistence in lifting morals of the students. He is the man with principles and he loves to interact with students. I distinctly remember the fact that even after taking over the Department Chair position, he was always easily approachable to me and sometimes stayed after hours to discuss the research progress. Without his persistent help and the financial support this thesis work would not have been possible.

I would like to express my sincere gratitude to Dr. Mingyu Lu for providing technical help and constant motivation during my Masters at UTA. He was always accessible to me, literally any time of the week. I would like to thank him for serving as supervising professor on my thesis defense. Special thanks to my supervising professor, Dr.Saibun Tjuatja for his approach and suggestions, which helped me a lot in my thesis.

This work would not have been possible without the technical support provided by Mr.Doug Reed from Spirent Communications. His curiosity and persistence for excellence always pushed me to new levels. He shaped my ability to understand the theory behind the Over-The-Air testing approach. He showed a great patience in constantly answering to my

queries and long chain of E-mails. He shared his thoughts quite frankly and mentored me throughout my work. I really appreciate the time and efforts he put into this work along with me. I will be always grateful to him for lending me the necessary technical equipments for my experiments.

This work is dedicated to my mother Chandrarekha, father Arjunrao, sister Jaswandi and my fiancée Anagha. Without their love and constant support, I would not have succeeded in my goal. They always trusted me and loved me unconditionally.

Finally, I would like to thank all my fellow graduate students and my research mates at WSRC. I will be always grateful to my dearest friends from UTA, Omkar Thakur, Gaurav Mogane, Abhishek Sabnis, Ashutosh Parulkar, Rahul Patil, Neelima Kalidindi, Minal Patankar and my beloved sister Sneha Chavan who have been like my family members in USA.

November 23, 2009

ABSTRACT

ANALYSIS OF THE SPATIAL CORRELATION MEASUREMENTS FOR THE MULTIPLE INPUT MULTIPLE OUTPUT (MIMO) CHANNEL USING ANECHOIC CHAMBER MEASUREMENT METHODOLOGIES TO EVALUATE OVER-THE-AIR (OTA) TESTING TECHNIQUES

Digvijay Arjunrao Jadhav, M.S

The University of Texas at Arlington, 2009

Supervising Professor: Dr. Jonathan Bredow.

There are numerous constraints in defining an Over-The-Air (OTA) test due to the practical hardware restrictions present in an anechoic chamber. It is necessary to evaluate the test signals used in OTA testing to verify that the real world multipath propagation can be recreated for OTA testing inside an anechoic chamber. The objective of this measurement is to check whether the parameter, 'Spatial Correlation' can be used to compare OTA test signals used in the MIMO OTA testing. Spatial Correlation has prime importance from the point of view of MIMO channel modeling. It's a key factor in determining the MIMO channel capacity.

The spatial correlation describes the correlation between the antenna elements. It is basically a function of the parameters such as system bandwidth, angle of arrival (AoA), power azimuth spectrum (PAS), antenna spacing and the antenna polarization effects.

In this work a quantitative analysis of spatial correlation measurements for MIMO channel is presented. A Laplacian PAS is used to model the angular spread of the signal

present at MS. This emulates the angular spread observed in the outdoor environments such as urban and rural areas. A practical MIMO OTA test set up is developed with reduced number of antenna elements to measure the spatial correlation at the receiver. The work mainly deals with the OTA design description using Anechoic Chamber Measurement Methodologies to evaluate the performance of the OTA signals used to generate narrow angle spread signals representing the cluster of a wideband frequency selective MIMO channel. Lab VIEW based automated measurement platform was developed in order to take the simultaneous measurements for the multiple receive elements. The measured data confirms the ability to replicate the real world multipath fading environment inside the chamber. The spatial correlation measurements technique allows us to distinguish between the MIMO propagation effects and the antenna effects. This has imperative merit while evaluating the MIMO OTA test signal used in throughput measurements. It is confirmed that the 3-component prefaded model emulates the angle spread observed in the spatial channel model.

TABLE OF CONTENTS

LIST OF ILLUSTRATIONS

Figure Page

LIST OF TABLES

CHAPTER 1

INTRODUCTION

1.1 MIMO Systems

Multiple Input and Multiple Output (MIMO) Communication Systems have drawn significant attention since 1990's. The principle ideas in this field were derived from the work by A.R. Kaye and D.A. George (1970) and W. van Etten (1975, 1976). In 1984 and 1986 Jack Winters and Jack Salz at Bell Laboratories published several papers on beam forming related applications. Arogyaswami Paulraj and Thomas Kailath proposed the concept of Spatial Multiplexing using MIMO in 1993. They received U.S patent for this innovation in 1994 [1]. Greg Raleigh and Gerard J. Foschini investigated [2] [3] [4] that the MIMO systems can achieve higher capacity than the Single Input Single Output Systems (SISO) which uses one antenna element both at Transmitter and Receiver. He proposed a system architecture which uses multiple antennas at both Transmitter and Receiver to achieve higher data rates. Later in 1998 Bell Labs demonstrated the first laboratory prototype of Spatial Multiplexing technology which is principle technology behind the improved data rates due to MIMO [4].

1.1.1 MIMO Configurations

Depending upon the number of antenna elements used at Transmitter/Receiver and the number of users the MIMO and be configured as follows:

1.1.1.1. Single Input Multiple Output (SIMO)

SIMO is a degenerated form of MIMO wherein the Transmitter has single antenna but the Receiver uses multiple antennas.

1.1.1.2 Multiple Input Single Output (MISO)

MISO is a degenerated form of MIMO wherein the Receiver has single antenna but the Transmitter uses multiple antennas.

1.1.1.3. Single user MIMO Techniques (SU-MIMO)

The higher data rates are obtained by carefully allocating the data streams to the multiple transmitting antennas. The Bell Laboratories Layered Space-Time (BLAST), Gerard J. Foschini (1996) is the pioneering architecture of this type [4]. The other techniques are Per Antenna Rate Control (PARC), Varanasi, Guess (1998) Chung, Huang, Lozano (2001) and Selective Per Antenna Rate Control (SPARC), Ericsson (2004)

1.1.1.4. Multi user MIMO Techniques (MU-MIMO)

In MU-MIMO, the network can allocate each antenna to the different users instead of allocating only single user as in single-user MIMO scheduling. (E.g. PU^2RC).

MU-MIMO is more feasible with low complexity mobiles having small number of antennas than SU-MIMO with high system throughput capability. Using this technology, the network can transmit user data through a codebook-based spatial beam or a virtual antenna.

The MIMO implementations suffer some practical limitations such as the physical antenna spacing at Transmitter and Receiver is different and usually at the Base Station (BS) the antennas are placed at multiple wavelengths apart from each other. Due to the limited space availability at the User Equipment (UE) advanced antenna design schemes needs to be considered for practical implementations.

Recently researchers are focusing on the multi-user multi-antenna MIMO system configurations. 3GPP and WiMAX standards are treating MU-MIMO as one of the candidate technology.

1.1.2. The Basics of MIMO

Figure 1.1 shows the Physical MIMO System Channel. The transmitter has multiple transmit antennas and proper scheduling of the data streams (T1, T2…Tn) helps in the transmission of signals. These signal streams go through a random channel gain matrix H which has multiple paths between multiple antennas of the transmitter and receiver. The path gains are represented by the individual path gains of h_{11}, h_{12},….., hmn. When the signal stream passes through the channel the noise N gets added into the signal stream. The received signal vector R is given by the MIMO System Model shown in equation 1.1.

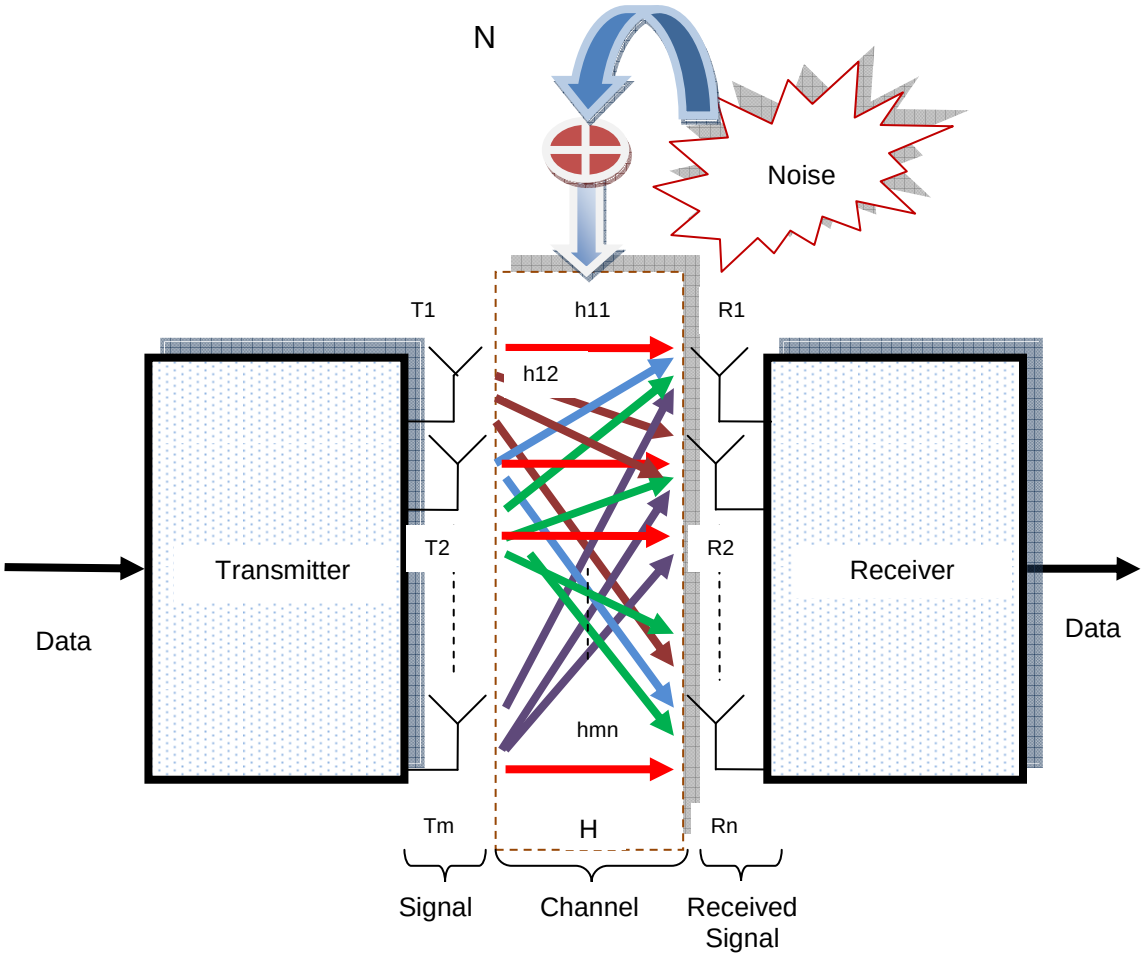

Figure 1.1 Representation of a Physical MIMO System Channel

$$R = H*T + N \quad (1.1)$$

Here R and T are the Receive and Transmit Signal vectors where H and N are Channel and Noise vectors. It is important to know the coefficients (path gains) of the transfer channel matrix H for decoding the signal steam. These coefficients are obtained from the defined training sequence [8].

1.1.3. Key Technology behind MIMO

There are three main modes of MIMO namely Precoding, Spatial Multiplexing and Diversity Coding.

1.1.3.1. Precoding

In this technique the transmitter does spatial processing of the signal at its end. In other words, it can be seen as the multi-layer beam forming technique at the transmitter. If the receiver sends the Channel State Information (CSI) back to the transmitter then this information can be used by the transmitter for precoding [8] [25]. For (single-layer) beamforming, the same signal is emitted from each of the transmit antennas with appropriate phase (and sometimes gain) weighting such that the signal power is maximized at the receiver input. In beamforming the constructive combining of the signal gain takes place which reduces the multipath fading effect. If the signal does not experience any scattering then beamforming results in a well defined directional pattern, but in typical cellular environment conventional beams are not a good analogy. When the receiver has multiple antennas, the transmitter beamforming cannot simultaneously maximize the signal level at the entire receiver antennas then precoding is used to combat this problem.

1.1.3.2. Spatial Multiplexing

In spatial multiplexing, a high rate signal is decomposed into multiple lower rate streams and each stream is transmitted from a different transmit antenna in the same frequency channel .Thus spatial multiplexing is advantageous in a way that it uses same channel to carry more than one spatial data stream over the same frequency simultaneously. When these signals

arrive at the receiver antenna array with sufficiently different spatial signatures, the receiver can separate these streams, by creating parallel channel streams which can be combined together by parallel to serial mapping. This is shown in figure 1.2.The original data stream 10001101 is decomposed into the multiple low data rate streams which carry a part of the original sequence. These streams are combined at receiver to regenerate the original sequence.

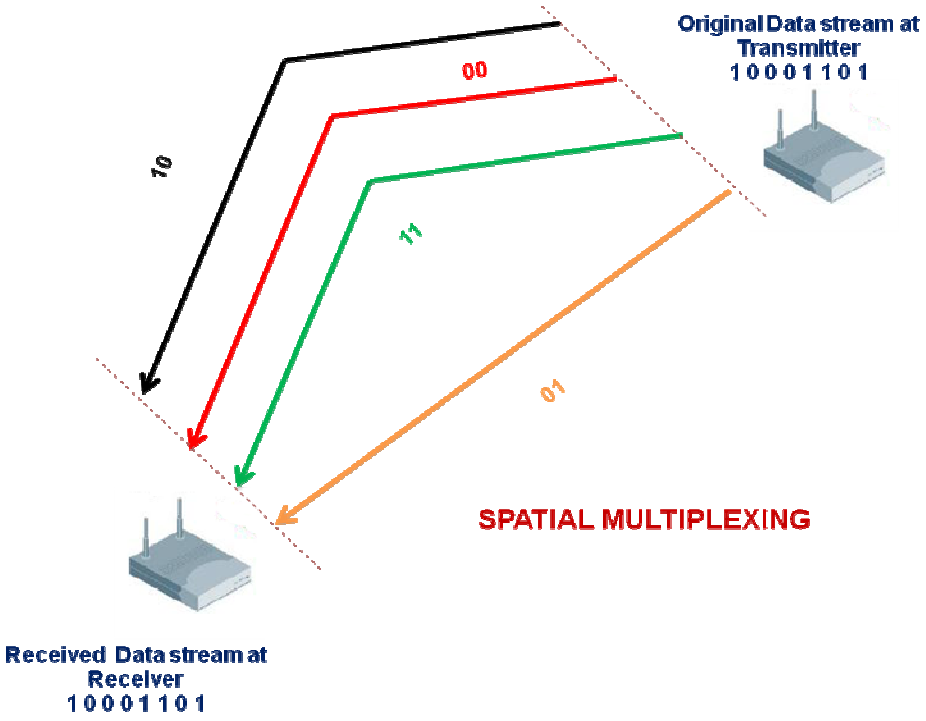

Figure 1.2 Representation of Spatial Multiplexing in MIMO System

The capacity of the channel with high Signal to Noise Ratio (SNR) can be increased significantly by using spatial multiplexing. The maximum number of spatial streams is bounded by the total number of antennas at the transmitter or receiver, whichever is the minimum.

The advantage of the spatial multiplexing over the precoding is that the transmitter does not require the knowledge of the channel [8] [25].

1.1.3.3. Diversity Coding

Diversity Coding techniques are useful when the transmitter does not have any knowledge about the channel. The diversity coding differs from the spatial multiplexing in a way that a single stream (unlike multiple streams in spatial multiplexing) is transmitted, but the signal is coded using techniques called space-time coding. The space –time encoder at the transmitter uses certain principles of full or near orthogonal coding. Diversity exploits the independent fading in the multiple antenna links to enhance signal diversity. As the transmitter does not have any channel knowledge there is no beamforming or array gain from diversity coding [8] [25].

If there is a trade-off on decoding reliability then the spatial multiplexing can be combined with diversity coding or else the spatial multiplexing can be combined with precoding to get the beam forming or array gain.

Apart from these techniques several other techniques like Smart Antenna techniques, Space-Time coding techniques do exist which essentially combines these basic functions of MIMO to obtain the desired reliability and the data rates in a given scenario.

1.2 Basics of the OTA Testing Techniques

In the previous section the advantages of MIMO configurations were discussed. Over-The-Air testing techniques evaluate the practical system performance and thus validate the qualitative benefits mentioned in the literature. It is necessary to estimate the radiated performance of the User Equipment (UE) by OTA techniques. The OTA measurements determine the figure of merits for air-interface technologies. Usually the OTA measurements are categorized as Total Radiated Power (TRP) measurements and the Total Isotropic Sensitivity (TIS) Measurements [8].

1.2.1 Essentials of TRP OTA Testing

The radiation characteristics of the antenna can be categorized in three principle regions namely Reactive Near-Field, Radiated Near Field and Far-Field.

The Reactive Near-Field region is typically within a few wavelengths of the antenna/DUT. The fields in this region are a combination of propagating electromagnetic waves and energy stored in electric (capacitive) or magnetic (inductive) fields. Any object introduced in this region changes the stored energy and thus affects the physical properties of the antenna (impedance, etc.)[26].

The Radiating Near-Field (*Fresnel*) region consists primarily of propagating RF energy, but in non-uniform directions.

The far-field (*Fraunhoffer*) region consists of propagating RF energy in coherent plane waves (or spherical wave front when viewed in 3-D). In this region E-M waves appear to be coming from a single point source [25].

1.2.2 Essentials of TIS OTA Testing

In order to get the Total Isotropic Sensitivity of the equipment under test (EUT), it is required to have a control on the base station (BS) power level or transmitter power level. The transmitter power level is reduced gradually and the bit error rate (BER) of the received signal at EUT is observed [8].The sensitivity test is carried out for various angles at EUT with respect to the base station antenna.

1.2.3 Essentials of MIMO OTA Testing

Unlike the TRP and TIS measurements for single input single output (SISO) system OTA testing techniques for MIMO Systems are much more rigorous due to the complexity involved in the data processing. As discussed in [8] if each antenna is considered individually and the measurements are carried out in MIMO test system then these measurements will essentially have uncorrelated data from each channel. This approach will not be useful to assess the overall EUT performance in the network. However in MIMO systems the emphasis should be given on the multiple antenna elements set-up and then the data should be collected such that every element either from receiver or transmitter will be active at all the time throughout the measurements. In order to get true sense of OTA performance testing, the

outdoor fading scenarios should be modeled correctly in the MIMO channel. Thus the Channel modeling plays important role in evaluating the OTA methodologies for MIMO systems.

1.3 Significance of Spatial Correlation Measurements for MIMO Channels

There are numerous constraints in defining an OTA test due to the practical hardware restrictions present in an anechoic chamber. In order to check the authenticity of the test signals used in the OTA testing we need a parameter which can give the qualitative analysis of the MIMO terminals being used. In this work the parameter 'Spatial Correlation' is used to compare OTA signals used for MIMO OTA testing.

The spatial correlation describes the correlation between the antenna elements. It is basically a function of the parameters such as system bandwidth, angle of arrival (AoA), power azimuth spectrum (PAS), antenna spacing and the antenna polarization effects.

Spatial Correlation has prime importance from the point of view of MIMO channel modeling. It's a key factor in determining the MIMO channel capacity. The estimated spatial correlation either at the transmitter or at receiver will allow us to compute the capacity and design the antenna array so that the capacity is maximized. For MIMO channels the capacity is inversely related to the spatial correlation values. Higher correlation values represent lack of multipath effect in channel. The capacity is high for lower correlation values.

The correlation coefficients can be used to determine the coefficients of the frequency selective channel matrix. The instantaneous channel capacity per unit bandwidth (in b/s/Hz) of the frequency selective fading MIMO channel employing *M* transmit and *N* receive antennas can be expressed as [6] ,

$$C = \frac{1}{B}\int_{B} \log_2 \det\left[I_N + \frac{SNR}{M} H(f) H^{\dagger}(f) \right] df \tag{1.2}$$

Where,

B = Signal Bandwidth

H (f) = The frequency-dependent transfer function matrix of dimension (N × M),

The superscript † stands for conjugate transposition

SNR = The signal-to-noise ratio

I_N = The (N × N) identity matrix

Now the frequency selective MIMO channel with M transmit and N receive elements can be given by the channel matrix H as follows [6] ,

$$H(\tau) = \sum_{l=0}^{L-1} \overrightarrow{H}_l \left(\delta(\tau - \tau l)\right)$$

(1.3)

Where, L denotes the number of resolvable multipath components determined by L = $[B\tau m]$ with B and τm denoting the signal bandwidth and the maximum excess delay, respectively. For the sampling rate of 1/B, the delays τl in (1.3) are related as τl = *l/B, l= 0, . . .* ,L − 1. $\overrightarrow{H}_l$, denotes the (N × M) complex channel matrix containing the fading coefficients at the τl delay given by [6],

$$\overrightarrow{H}_l = \begin{bmatrix} h_{11}^{l} & h_{12}^{l} & \ldots\ldots & h_{1M}^{l} \\ h_{21}^{l} & h_{22}^{l} & \ldots\ldots & h_{2M}^{l} \\ \cdot & & & \\ \cdot & & & \\ \cdot & & & \\ h_{N1}^{l} & h_{N2}^{l} & \ldots\ldots & h_{NM}^{l} \end{bmatrix}$$

(1.4)

The spatial correlation for the MIMO channel can be expressed in terms of the spatial correlation measured at transmitter and at receiver. It is shown below [6],

$$\mathbf{R}_{MIMO} = \mathbf{R}_{TX} \otimes \mathbf{R}_{RX}$$

(1.5)

Where, ⊗ represent the Kronecker product. The correlation matrix for each resolvable delay is given by [6],

$$\mathbf{R}_l = \mathbf{R}_l^{Tx} \otimes \mathbf{R}_l^{Rx}$$

(1.6)

Where the complex correlation coefficients at Tx and Rx are given by [6],

$$\mathbf{R}_l^{Tx} = \begin{pmatrix} r_{l,11}^{Tx} & r_{l,12}^{Tx} & \cdots & r_{l,1M}^{Tx} \\ r_{l,21}^{Tx} & r_{l,22}^{Tx} & \cdots & r_{l,2M}^{Tx} \\ \vdots & \vdots & \ddots & \vdots \\ r_{l,M1}^{Tx} & r_{l,M2}^{Tx} & \cdots & r_{l,MM}^{Tx} \end{pmatrix}$$

$$\mathbf{R}_l^{Rx} = \begin{pmatrix} r_{l,11}^{Rx} & r_{l,12}^{Rx} & \cdots & r_{l,1N}^{Rx} \\ r_{l,21}^{Rx} & r_{l,22}^{Rx} & \cdots & r_{l,2N}^{Rx} \\ \vdots & \vdots & \ddots & \vdots \\ r_{l,N1}^{Rx} & r_{l,N2}^{Rx} & \cdots & r_{l,NN}^{Rx} \end{pmatrix}$$

(1.7)

And the correlation coefficients between a pair of channels for i^{th} and j^{th} transmit elements received on n^{th} receiver element is given by (1.8)

$$r_{l,ij}^{Tx} = \frac{E\left[h_{ni}^{l} h_{nj}^{l^*}\right] - E\left[h_{ni}^{l}\right] E\left[h_{nj}^{l^*}\right]}{\sqrt{\left(E\left[\left|h_{ni}^{l}\right|^2\right] - \left|E\left[h_{ni}^{l}\right]\right|^2\right)\left(E\left[\left|h_{nj}^{l}\right|^2\right] - \left|E\left[h_{nj}^{l}\right]\right|^2\right)}}$$

(1.8)

Similarly for the correlation coefficients between a pair of channels for i^{th} and j^{th} receiver elements transmitted by the m^{th} transmitter element is given by (1.9)

$$r_{l,ij}^{Rx} = \frac{E\left[h_{im}^{l} h_{jm}^{l^*}\right] - E\left[h_{im}^{l}\right] E\left[h_{jm}^{l^*}\right]}{\sqrt{\left(E\left[\left|h_{im}^{l}\right|^2\right] - \left|E\left[h_{im}^{l}\right]\right|^2\right)\left(E\left[\left|h_{jm}^{l}\right|^2\right] - \left|E\left[h_{jm}^{l}\right]\right|^2\right)}}$$

(1.9)

Now, these coefficients can be used to get the channel matrix coefficients by [6] (1.10),

$$\mathrm{vec}(\tilde{\mathbf{H}}_l) = \mathbf{R}_l^{1/2}\,\mathrm{vec}(\mathbf{H}_l^{w})$$

(1.10)

Where, the NM × NM matrix $\mathbf{R}_l^{1/2}$ is obtained by factoring the total correlation matrix R_l and the $\mathbf{H}_l^{w}$ represents the i.i.d white Gaussian random matrix for each tap. Thus, these channel coefficients are used to estimate the channel capacity using (1.2).

In this work a quantitative analysis of spatial correlation measurements for MIMO channel is presented. A practical MIMO OTA test set up is developed to measure the spatial correlation at the receiver. The work mainly deals with the OTA design description using Anechoic Chamber Measurement Methodologies to evaluate the performance of the OTA signals used to generate narrow angle spread signals representing the cluster of a wideband MIMO channel. Lab VIEW based automated measurement platform was available for single element radiation pattern measurements. This platform was modified in order to take the simultaneous measurements for the multiple receive elements. The RF Channel Emulators are used to replicate the real world multipath fading scenarios observed in MIMO channels. These faders were supplied by the Spirent Communications. These faders generate the rich scattering environment observed in the MIMO channels. They can generate the spatial channel models which take into account the spatio-temporal characteristics of the MIMO Channel. The output signals from these faders are always uncorrelated.

Further chapters of this work are organized as follows: Chapter 2 gives an overview of the Spatial Channel Models (SCM) used in MIMO systems. It demonstrates the importance of spatial correlation in SCM by providing a detailed analysis of different channel models.

Chapter 3 mainly describes the Measurement set-up and its components. The development of the test system and its automated measurement platform using Lab VIEW program is thoroughly discussed. The working of the RF Channel Emulator is described in brief.

Results of the measurements and there analysis is documented in Chapter 4. Chapter 5 mainly concludes the experimental results and discusses the findings. It also gives insight to the possible extension of this work in order to further improve the measurement results. The data analysis was carried out using MATLAB and its packages. The document ends with appendix section which provides the technical specifications on the instruments used in this work.

CHAPTER 2

BACKGROUND INFORMATION

2.1 Effects of Multiple Antenna Elements

The multiple-input multiple-output (MIMO) antenna systems have a potential to explore the data rates available in long term evolution (LTE). It is mentioned in [8] [24] [25] that the MIMO has certain advantages over the SISO system due to its ability to utilize the spatio-Polarimetric dimensions of the radio channel. The functions of MIMO explained in [25] focuses on the coherent case where the channel is known at the receiver and transmitter does not have any information about the channel.

Precoding uses the spatial degrees of freedom to generate multilayered beamforming which basically reduces the co-channel interference by suppressing the undesired signal. This technique improves the capacity of the system drastically. The Spectral Efficiency is improved by the Spatial multiplexing gain which uses the single frequency band to transmit multiple spatial data streams simultaneously without additional power requirements. Link reliability can be improved by diversity coding which provides multiple (ideally) independently fading signal paths between transmitter and receiver. Although it looks promising to achieve higher data rates using these gain techniques available in MIMO channel, it requires a very sophisticated channel model to realize such high end performance expected in LTE. The performance of the MIMO channel can be affected by the antenna element at the UE, its position and its orientation. In order to study these effects it is required that the channel should be modeled to insure the exact representation of the real world test condition [15].

2.1.1. Channel Models for OTA Testing

Study has shown that the current Radio Channel (SISO System) does not represent all dimensions of the MIMO channel [9][13][14][15].

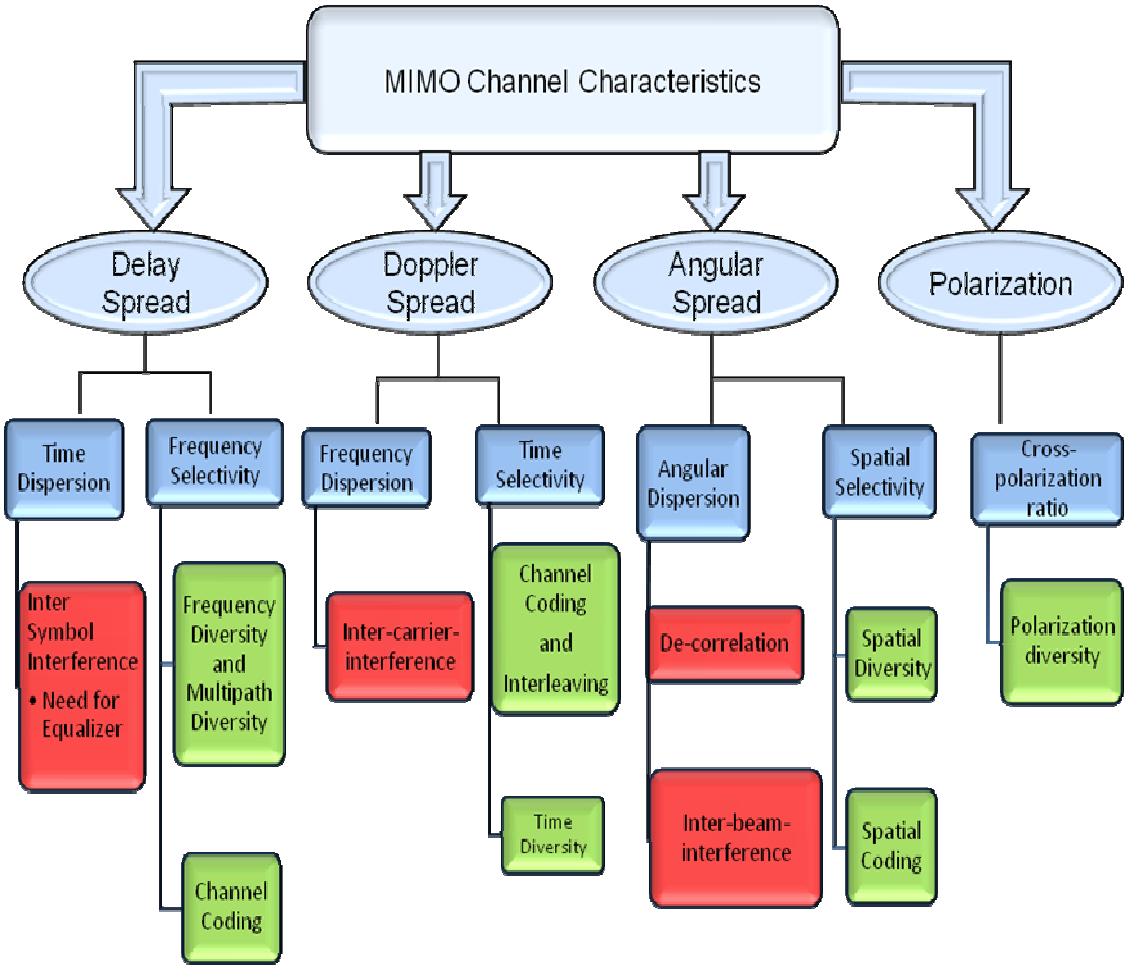

Figure 2.1 The Characteristics of MIMO Channel

Prior to MIMO testing ,the available Radio channel models considered only two dimensions of the channel modeling namely, 1) Large Scale parameters: Path loss and Shadowing Effects (Power Scaling) and 2) Dispersion Characteristics of the signal : Delay Spread and Doppler Spread. The effects of the antenna pattern and the orientation of the UE

were neglected in previous scenarios. In a MIMO channel the Angular (spatial) dispersions and Polarimetric dispersions contains the embedded information regarding the Delay spread and Doppler Spread. These dispersions should be considered in channel modeling to preserve the realistic channel behavior. Different aspects of MIMO Radio channel discussed in [16] show that the MIMO channel should reflect all the four dimensions of the channel namely: Space, Time, Frequency and Polarimetric characteristics.

Figure 2.1 represents these four dimensions of the MIMO channel and there effects on the MIMO performance. The impact of these dimensions can be either constructive or destructive. A well-designed channel model will exploit these degrees of freedom to achieve desired performance. Also several techniques are listed in the figure in order to alleviate the effect of these dispersions on the channel performance. The four types of the dispersions observed in the MIMO channel are given in figure 2.1. They significantly affect the throughput of the system. These four dimensions are interdependent and they give rise to the propagation conditions shown in figure 2.2 (a), (b) and (c). The MIMO channel model should have all the properties included in figure 2.2. [16][15]

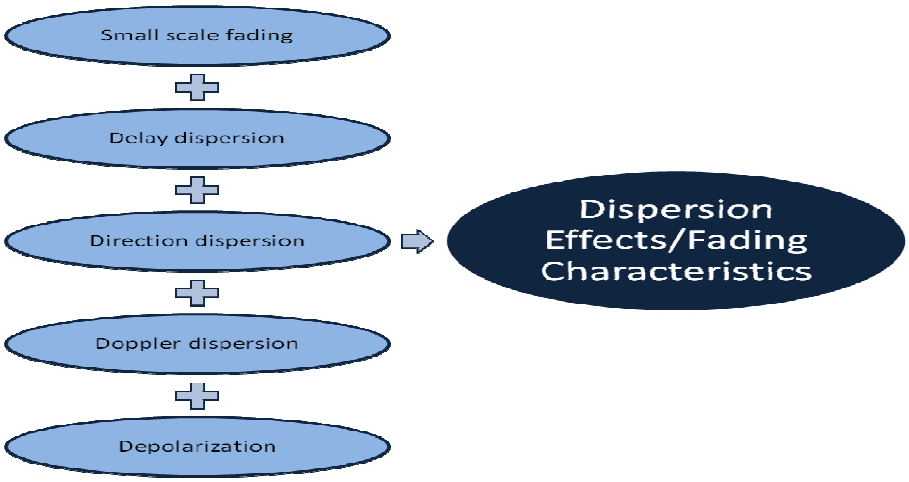

(a)

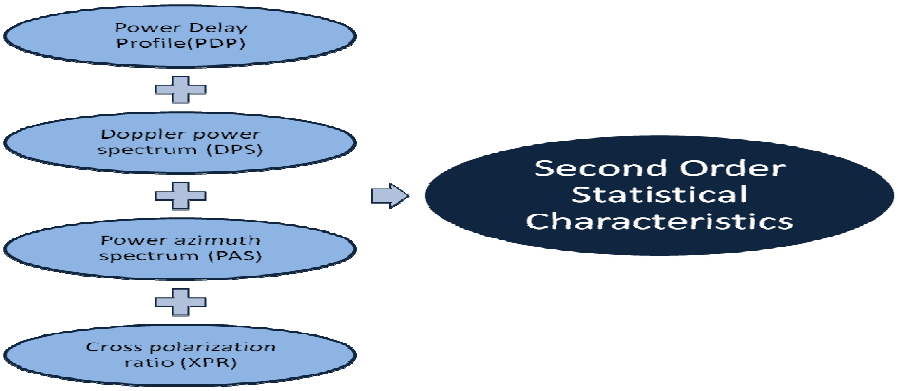

(b)

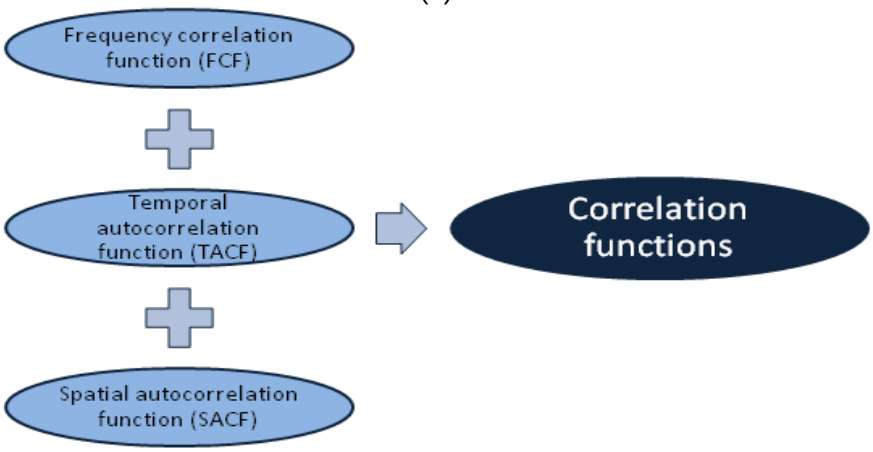

(c)

Figure 2.2 (a), (b) and (c) Properties of MIMO propagation

As mentioned in [8] and [16] in order to assess the performance of the MIMO link we have to measure the full terminal performance .Throughput gives the overall figure of merit for MIMO link .It takes into account all the dynamic behaviour of the whole radio link including the radio channel ,antennas , RF and signal processing. Thus it becomes essential to distinguish between the propagation and the antenna array effects. If the model can investigate the effects of these two components distinctly then it is possible to examine the propagation with different antenna configurations. This requirement makes all the correlation matrix based channel models unsuitable for OTA testing [16] [15]

As mentioned in chapter 1 different MIMO modes (Precoding, Spatial Multiplexing, Diversity Gain) exploit all these dimensions of the MIMO channel to achieve better performance. Thus to compare different MIMO modes it is necessary to model the phase relations and the correlation between the signals on different antenna elements.

2.1.2 Spatial Channel Models for MIMO OTA testing

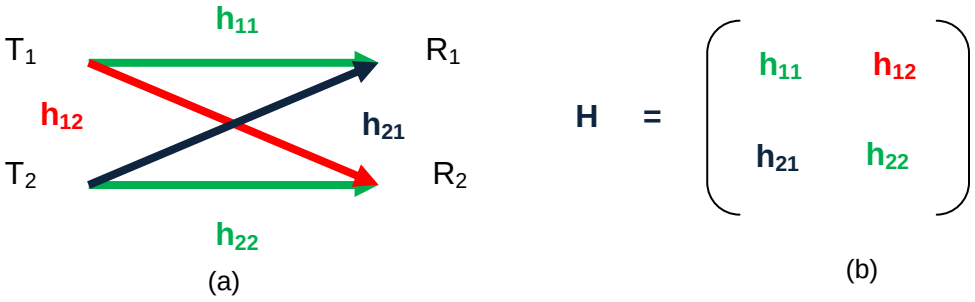

Figure 2.3 A 2x2 MIMO System. (a) 2x2 MIMO Antenna Configuration and (b) Complex Channel matrix for 2x2 MIMO System

It was established in the last session that the correlation plays important role in comparing the different channel modes for MIMO testing. Figure 2.3 (a) shows a 2x2 MIMO antenna configuration where the four interconnecting paths h_{11}, h_{12}, h_{22}, h_{21} represent the gain and phase characteristic between the transmitter and receiver equipment along those paths. The complex channel matrix is shown in figure (b).

The output vector Y, for this configuration can be written by using equation (1.1) as follows:

$$Y = \begin{pmatrix} r1 \\ r2 \end{pmatrix} = \begin{pmatrix} h11 & h12 \\ h21 & h22 \end{pmatrix} \begin{pmatrix} T1 \\ T2 \end{pmatrix} + \begin{pmatrix} n1 \\ n2 \end{pmatrix} \quad (2.1)$$

Where, n_1, n_2 represent the noise vector values. Now the correlation between the transmit antennas [29] can be written as follows:

$$\rho(tx) = \frac{|2\mathrm{Re}(h11\ h12^*)|^2}{(1 - |h11|^2 - |h12|^2)} \quad (2.2)$$

Similarly the correlation at the receive antennas is given by:

$$\rho(rx) = \frac{|2\mathrm{Re}(h11\ h21^*)|^2}{(1 - |h11|^2 - |h12|^2)} \quad (2.3)$$

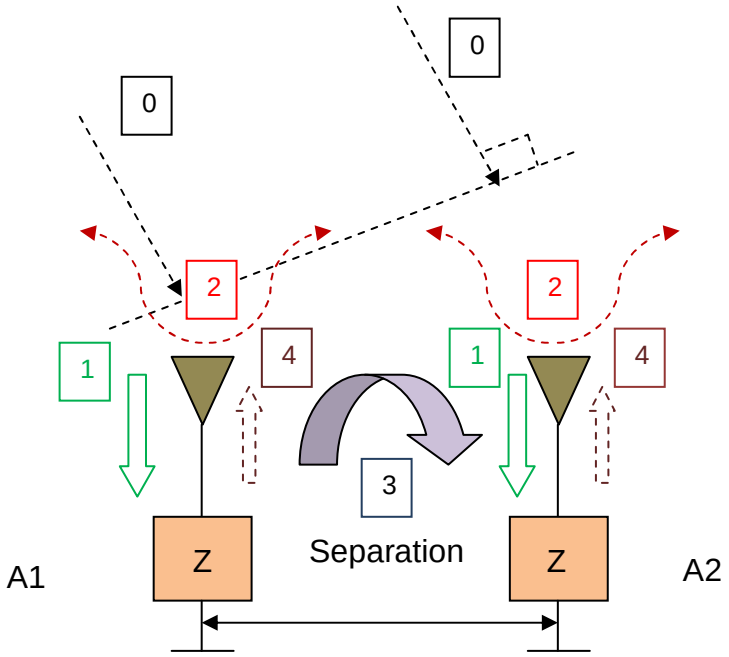

Figure 2.4 Effect of Coupling in receiving mode

It is evident that the correlation factor depends on the antenna reflection factor (h_{11}) and the antenna coupling factor (h_{12}). When two antenna elements are placed side by side and a plane wave is incident on them then the coupling between these two antennas plays an important role in receiving mode [26]. This receiving mode phenomenon is explained in figure 2.4.

The plane wave (0) incident on the antenna element A1 induces current on that element and the part of the signal is re-scattered by the element (2) in the free space. Some part of it will be directed to antenna A2 (3) due to the mutual coupling between the elements and rest of the part will go to the feed. At antenna A2 (3) will be added vectorially with (0). The A2 will also re-scatter some signal (2) incident upon it and the remaining part will travel to the feed (1). The distance between the elements will change the amount of coupling (3) between the elements. It is evident that the coupling between the elements modifies the current distribution along the antenna element and eventually it modifies the radiation pattern of the elements. Several impedance matching techniques are used to minimize the backscattered wave (2). Thus the mutual coupling between the antennas affects correlation of the received signal. It has been observed that the mutual coupling can have constructive as well as destructive effects on the performance of the MIMO channel.

All these aspects of the channel modeling are considered in the Geometry–based Stochastic Channel Models (GSCM) [16]. These models illustrate the multipath effects observed in the certain environmental conditions such as Urban, Sub-urban, Rural etc. Out of the available models in this family, Extended Spatial Channel Model (SCME) [9] is selected as the working assumption for the study and analysis [14], [13].

2.1.3 Basics of Extended Spatial Channel Model (SCME) for MIMO OTA testing

The extended spatial channel model (SCME) [13], is accepted as the working assumption in 3GPP. The angular parameters of the BS and MS are defined in this channel.

These specifications are shown in figure 2.5 and the angles measured in clockwise directions are considered negative. [13]

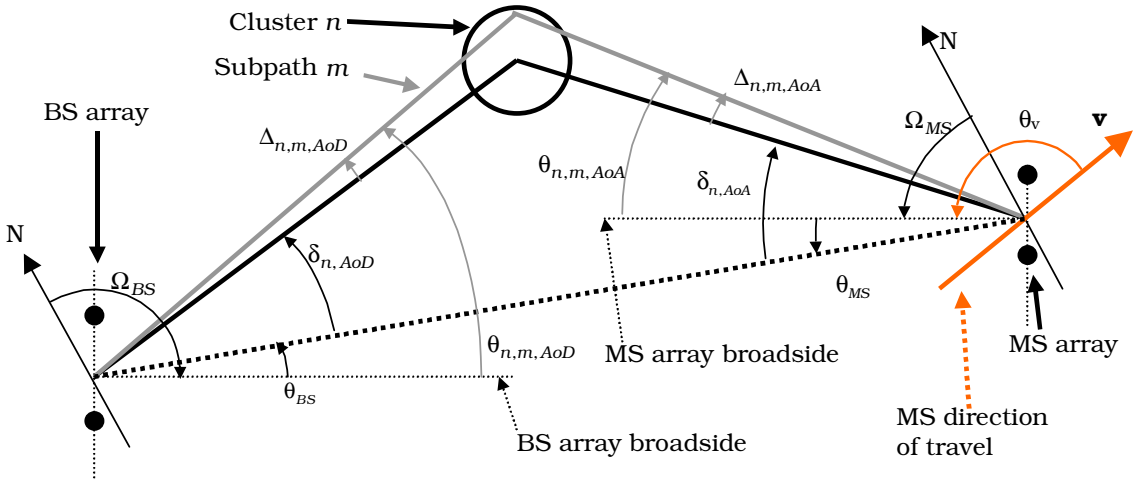

Figure 2.5 BS and MS angular parameters in SCME [13]

The angular parameters shown in figure 2.5 are defined as follows [13]:

Ω_{BS} BS antenna array orientation, defined as the difference between the broadside of the BS array and the absolute North (N) reference direction.

θ_{BS} LOS AoD direction between the BS and MS, with respect to the broadside of the BS array.

$\delta_{n,AoD}$ AoD for the nth (n = 1 … N) path with respect to the LOS AoD θ_0 .

$\Delta_{n,m,AoD}$ Offset for the m^{th} (m = 1 … M) sub path of the nth path with respect to $\delta_{n,AoD}$.

$\theta_{n,m,AoD}$ Absolute AoD for the m^{th} (m = 1 … M) sub path of the nth path at the BS with respect to the BS broadside.

Ω_{MS} MS antenna array orientation, defined as the difference between the broadside of the MS array and the absolute North reference direction.

θ_{MS} Angle between the BS-MS LOS and the MS broadside.

$\delta_{n,AoA}$ AoA for the nth (n = 1 … N) path with respect to the LOS AoA $\theta_{0,MS}$.

$\Delta_{n,m,AoA}$ Offset for the m^{th} (m = 1 … M) sub path of the n^{th} path with respect to $\delta_{n,AoA}$.

$\theta_{n,m,AoA}$ Absolute AoA for the m^{th} (m = 1 … M) sub path of the nth path at the MS with respect to the BS broadside.

v MS velocity vector.

θ_{v} Angle of the velocity vector with respect to the MS broadside: θ_{v} =arg (v).

The angular dispersion is thus modeled in the channel to maintain the necessary spatial-temporal characteristics of the MIMO channel. These channel models are suitable for wideband cellular channels. The multipath scenario can be reproduced in the chamber with the help of these models. The signals from the clusters are characterized by the narrow Angle Spread (AS) at particular Angle of Arrival (AoA) and delay. The important characteristic of a multipath signal is that the channel has frequency selective behavior with each delay having unique spatial attributes.

2.2 Analysis of Spatial Correlation Measurement Technique

The fading observed in radio propagation channel is caused by the interference between the multiple copies of the transmitted signal arriving at receiver with different power levels and delays. It affects the amplitude and phase of the signal. The time dispersions and the angular dispersions observed in MIMO radio channel induce the small scale fading effects along with the signal distortion. Due to the multipath propagation, the different versions of the transmitted signal arrive at the receiver with the exponentially decreasing power levels and delays which are increasing exponentially with time [20]. Usually the power delay profile model is used to represent these multipath characteristics of the channel. Figure 2.6 shows such a power delay profile of a multipath signal.

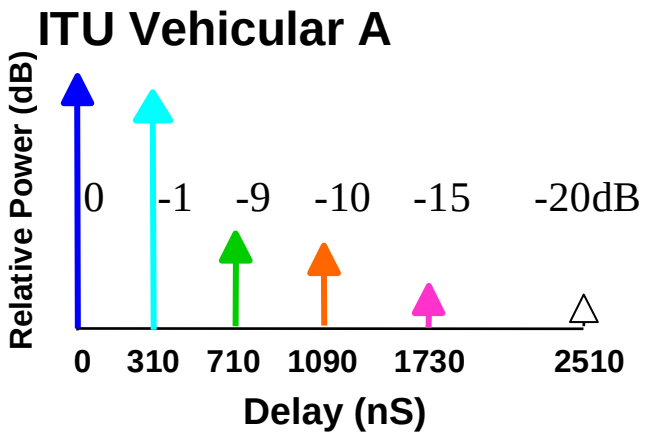

Figure 2.6 Power Delay Profile (PDP) Example [20]

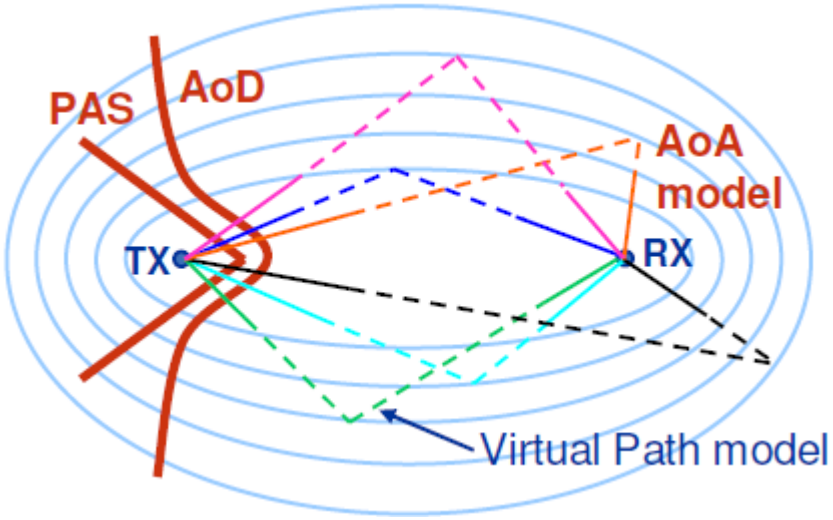

Figure 2.7 Example of a Spatial Channel Model [20], Top View

The spatial aspects of the signal path are incorporated in the SCM by an Angle of Departure (AoD) and Angle of Arrival (AoA) as shown in the figure 2.7. The signal will not follow the exact course shown by the virtual path model between the transmitter (BS) and the receiver (MS) but its angular properties at BS and MS will be modeled in the channel. Thus it is possible to define the delay and phase in SCM so that the power delay profile model can be used effectively for the analysis.

The *first-order* statistics of the multipath propagation involve characterizing the fading processes with a probability density function. In order to study the *second-order* statistics like autocorrelation and correlation measurements it is important to consider the shape factors of the multipath signal [28]. These shape factors are derived from the angular dispersion of the signal. The shape factor angular spread (σ) is a measure of how multipath concentrates about a single azimuthal direction of arrival. The calculation for such angular –spread (σ) is given in [13].

In order to model the exponentially distributed relative powers and the delays observed in power delay profile, it is recommended [13] [9] to use the Laplacian distribution and the Uniform distribution to model the per-path Power Azimuth Spectrum (PAS) at the MS. The Laplacian distribution governs the difference between two independent identically distributed exponential random variables. Laplacian PAS models the angular spread observed in the outdoor propagation environments like rural and urban areas. Equation (2.4) and (2.5) describes the continuous PAS at the MS.

$$PAS = \frac{Q}{(\sqrt{2}).\sigma} \exp\left[\frac{-\sqrt{2}|\theta - \phi|}{\sigma}\right] \tag{2.4}$$

Where,

$$Q = \frac{1}{erf\left[\frac{x}{(\sqrt{2})\sigma}\right]} \tag{2.5}$$

Assuming an omni directional antenna gain for the MS then the per-path Laplacian PAS value for an incoming AOA $\bar{\theta}$ and RMS angle-spread σ, at an angle θ is given by [13] equation (2.6).

$$P(\theta,\sigma,\bar{\theta}) = N_o \exp\left[\frac{-\sqrt{2}\left|\theta-\bar{\theta}\right|}{\sigma}\right] \tag{2.6}$$

Where both angles $\bar{\theta}$ and θ are given with respect to the boresight of the antenna elements. It is assumed that orientations of all antenna elements are aligned. Also, P is the average received power and N_o is the normalization constant given by (2.7) [13].

$$N_o^{-1} = \int_{-\pi+\bar{\theta}}^{\pi+\bar{\theta}} \exp\left[\frac{-\sqrt{2}\left|\theta-\bar{\theta}\right|}{\sigma}\right] d\theta \tag{2.7}$$

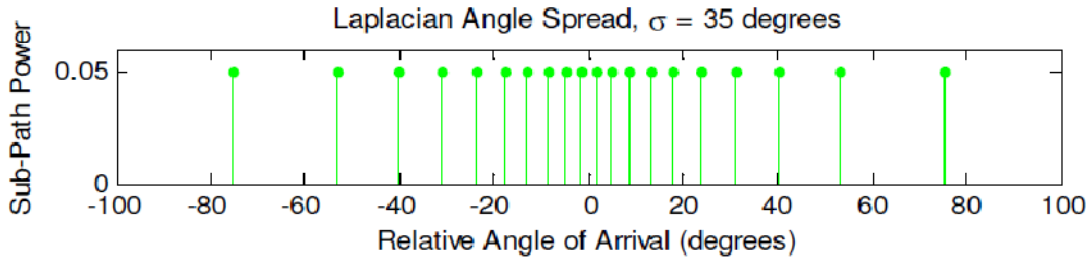

Figure 2.8 Path Model used in SCME [20] [9]

A discrete distribution with 20 equal powered sub-path sinusoids to represent each path is described in figure 2.8 [20] [9]. SCME uses this path model and here the AoDs and AoAs of the sub-paths are distributed non-linearly to emulate a Laplacian Power Azimuth Spectrum (PAS).

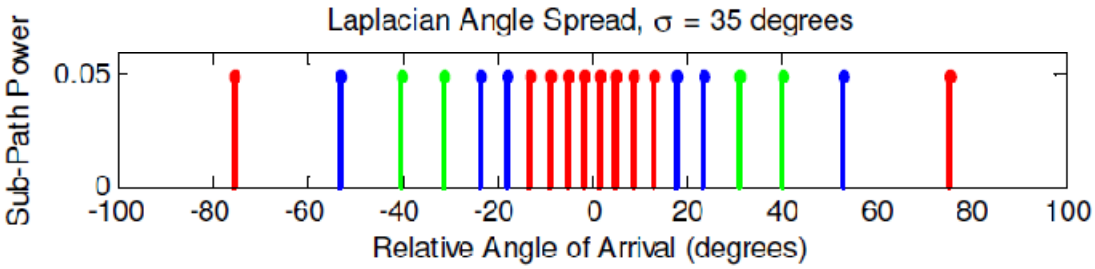

Figure 2.9 Path Model used in SCME (including mid paths) [20] [9]

In order to accurately represent the frequency de-correlation for wider-bandwidth channels the SCME extension includes the mid-paths as shown in figure 2.9 by the colors red, blue, and green, which indicate small relative delays of 0, 12.5, and 25 μs, with corresponding relative powers of 0.5, 0.3, and 0.2 [20]. The path model with more path components (Figure 2.8) is used in this work for the spatial correlation measurement analysis as it avoids errors due to quantizing.

2.2.1 Spatial Correlation analysis using SCME path model

The spatial correlation with the complex antenna patterns has the following form,

$$\rho(d) = \int_0^{2\pi} \mathrm{Gi}(\phi) * \mathrm{Gj}(\phi) * \mathrm{p}(\phi) \mathrm{e}^{(-\mathrm{j}2\pi d \cos(\phi)/\lambda)} d\phi \bullet \left[\int_0^{2\pi} \mathrm{Gi}(\phi) * \mathrm{Gi}(\phi) * \mathrm{p}(\phi) d\phi \bullet \int_0^{2\pi} \mathrm{Gj}(\phi) * \mathrm{Gj}(\phi) * \mathrm{p}(\phi) d\phi \right] \tag{2.8}$$

Where, the G_i and G_j are the antenna gains and the P (ϕ) is the probability distribution function (PDF) of the signal and d is the separation between the two elements. A more simplified version for spatial correlation using a continuous PAS is given by the equation (2.9). Its equivalent discrete version is shown in equation (2.10)

$$\rho(d) = \int_{-4\pi+\phi_a}^{4\pi+\phi_a} \mathrm{p}(\phi_i - \phi_a) \, \mathrm{e}^{(\mathrm{j}2\pi d \sin(\phi_i - \phi_a)/\lambda)} d\phi_i \tag{2.9}$$

$$\rho(d) = \frac{1}{M}\sum_{i=1}^{M} \mathrm{e}^{(\mathrm{j}2\pi d \sin(\phi_i - \phi_a)/\lambda)}$$

(2.10)

SCME defines the angle spread at BS to be 2^0 and 35^0 for the MS [13]. As the angle spread will govern the correlation between the antenna elements at the link end, it is intuitive to check the correlation for the two antenna elements as a function of the mean angle of arrival (AoA) with respect to broadside of the antenna array.

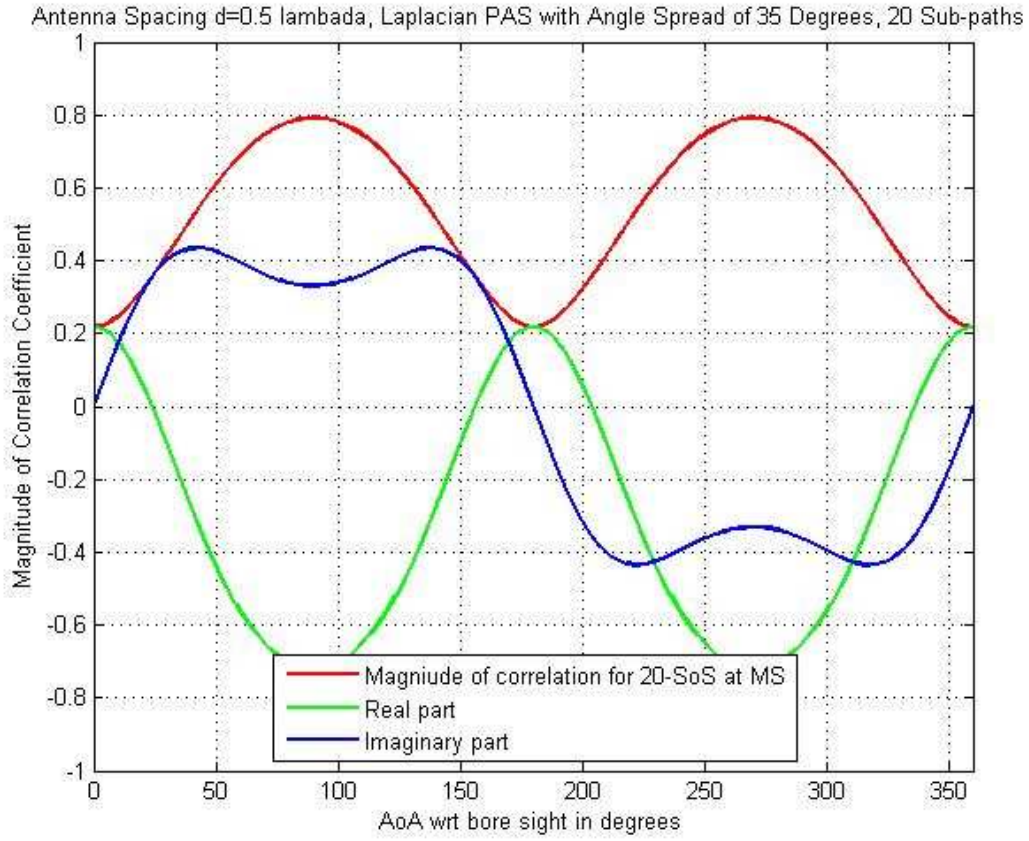

Figure 2.10 Azimuthal correlation for MS antenna

The figure 2.10 shows the simulation result for spatial correlation at MS using 20 sub-path sinusoids (SOS) having Laplacian PAS for 35^0 angle spread (σ).This method is used in [19]

and [20]. It is evident from mutual coupling phenomenon that the correlation will change based on the distance between two elements. For the analysis purposes the separation between two elements is chosen as half wavelength. Sometimes antennas at MS may be cross polarized and thus the spacing between the elements can be even less than half wavelength. Considering the tight specifications on the available space at MS the value chosen for the spacing between the elements is the practical one.

Similarly the spatial correlation for BS with Laplacian PAS for 2^0 angle spread (σ) is shown in figure 2.11. Typically the antenna elements at the BS are several wavelengths apart and the narrow angular spread represents higher magnitude of correlation than the one at MS.

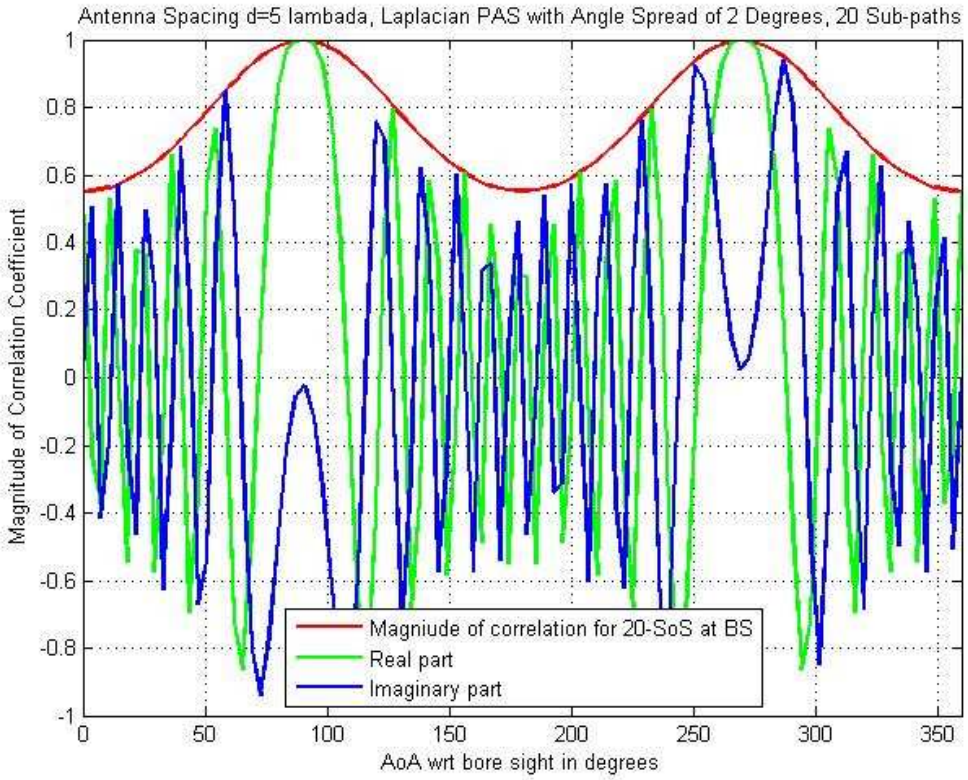

Figure 2.11 Azimuthal correlation for BS antenna

The effect of spacing'd' can be clearly observed in figure 2.11. As the spacing between the elements increases, the phase shift between the elements also increases [19] [20].

The narrow angular spread at the BS is due to the fact that most of the scatterers are positioned far from the BS. However the large numbers of local scatterers surrounding the MS give rise to the wider angle spread. If BS antennas are placed close to each other then it will result in high channel correlation but fortunately at BS enough area is available for antenna spacing. For practical antenna spacing available at MS, in order to get low channel correlations the observed wider angle spreads are suitable.

Generating these 20 sub-paths signals for over-the-air (OTA) testing is a very complex process. Also it will require placing these many individual probes in the chamber and it won't be cost effective. In order to carry OTA testing in the chamber it is important to generate a test signal which will faithfully represent the path model. Moreover if these many elements are present in the chamber then the chamber sensitivity will be affected i.e. the reflection from these elements and the structure supporting them will degrade the available RF quiet zone in the chamber. Hence it is challenging to reduce the number of probes placed in a chamber and still get a faithful representation of all the multipath attributes of the test signal. This technique achieves this goal by using only a subset of the 20 sinusoids with proper design.

The figure 2.12 shows 3-component model as a subset. This sub set uses 3-sinusods with specific AoA and relative power weightings to obtain a good match for the 20 sub-path case.

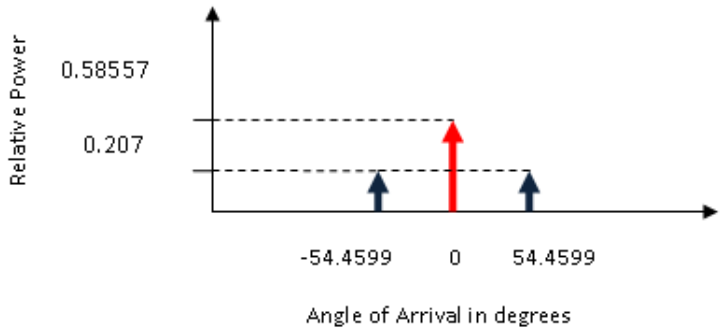

Figure 2.12 3 – component model

Using this 3-component model the spatial correlation is calculated at every AoA. The figure 2.13 shows the magnitude plot for the spatial correlation obtained at MS using 3-component model. The model maintains the 35^0 AS at MS and gives a good match for both amplitude and phase correlation obtained in 20 sub path model. The phase and amplitude correlation is showed in figure 2.14 [19] [20].

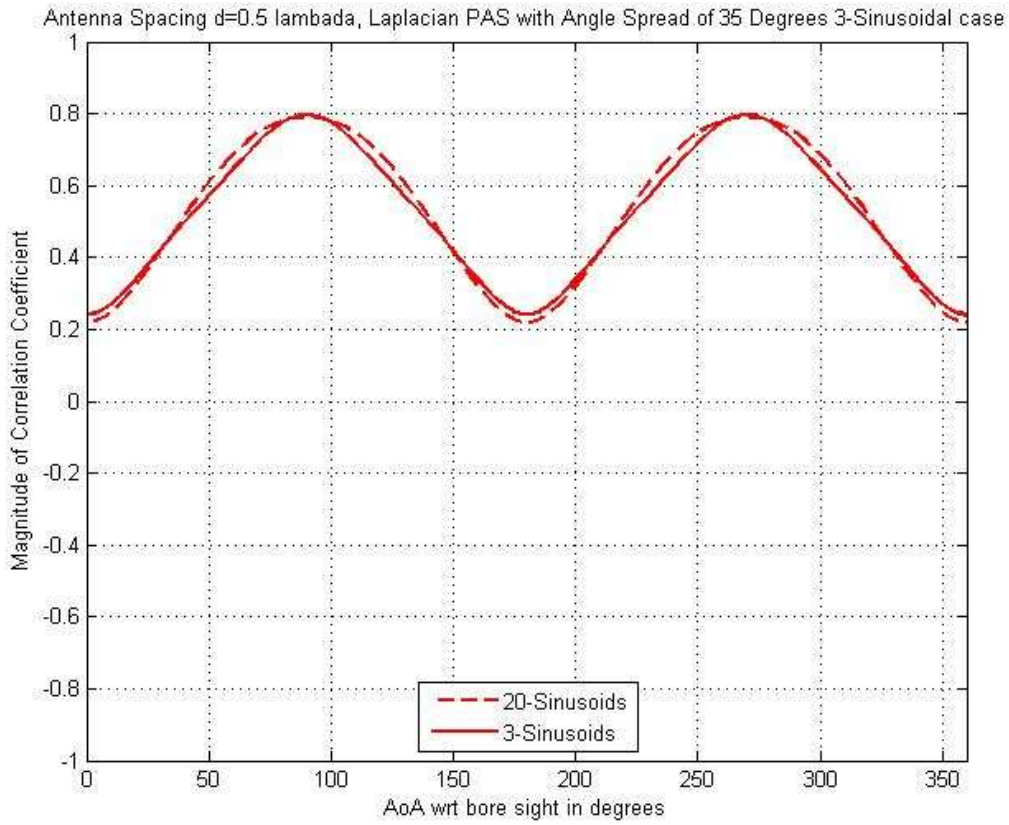

Figure 2.13 Matching the correlation at MS with 3 Sinusoidal case

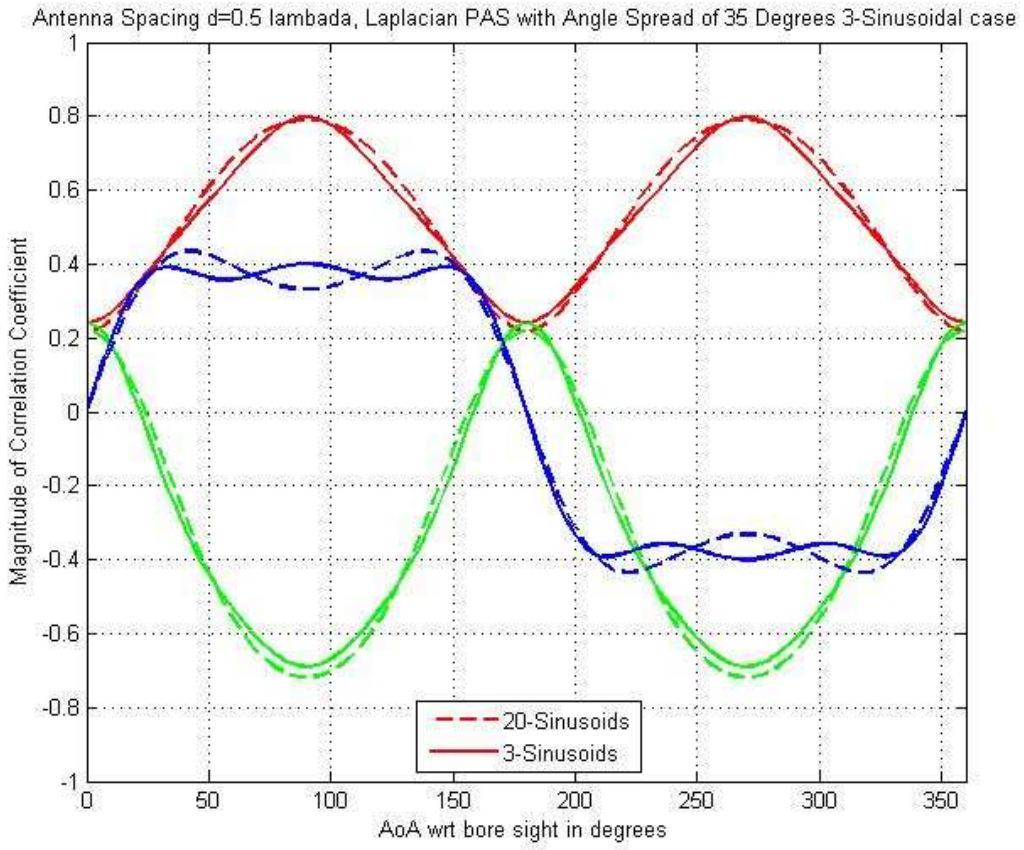

Figure 2.14 Phase characteristics using the 3 Sinusoidal case

Although 3- component model with unfaded sinusoids seems to be a good match for the 20 sub-path model, it is necessary to measure its *first-order* statistics i.e. the CDF or *second-order* statistics like Autocorrelation of the signal to investigate that, whether the multipath fading statistics are preserved by the test signal or not.

The autocorrelation for sum of sinusoids case as a function of lag distance is shown in figure 2.15. It can be seen that the autocorrelation is dramatically different than the ideal value represented by the 0^{th} order Bessel function. The autocorrelation for ideal SCM is realized by using the uniformly spaced AoA of 20 sub-path model having Laplacian PAS at MS with the AS of 35^0. Also the autocorrelation for the 3-equal power components with uniformly spaced angle of arrival is shown. From figure 2.15 it is clear that the unfaded 3-component Sum of Sinusoids

model will not represent the fading scenario. It should either require more number of SOS or a set of small number of components to be prefaded so as to obtain a good match to the ideal values[18][19][20].

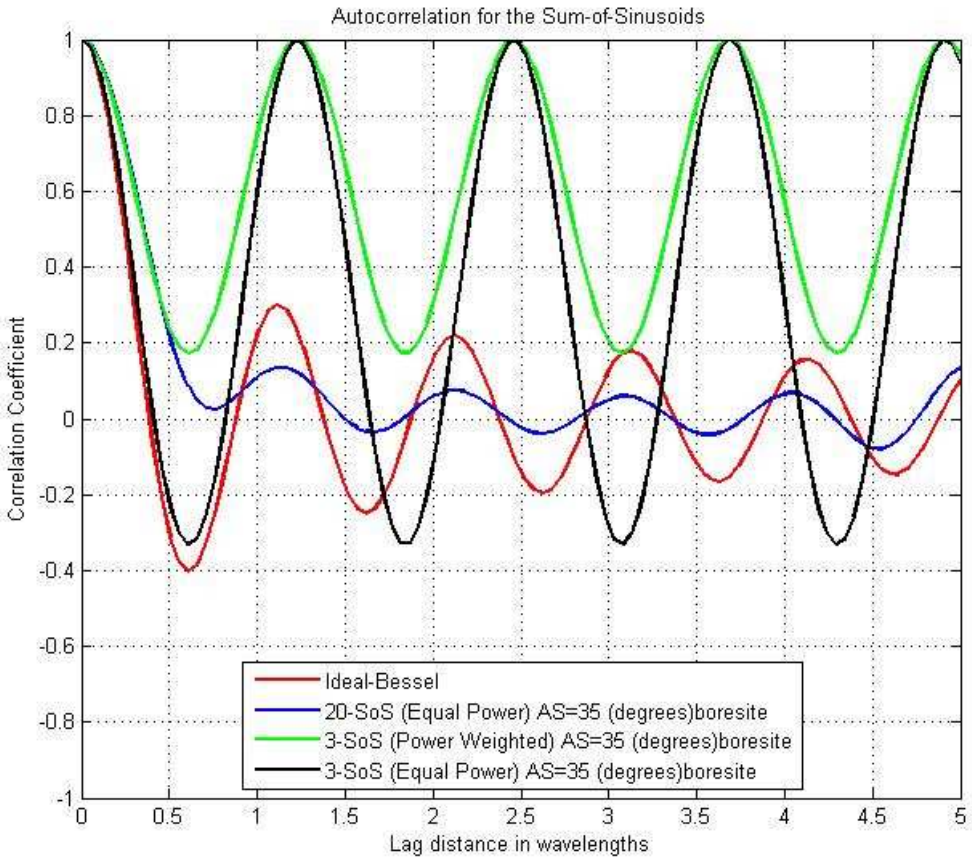

Figure 2.15 Signal Autocorrelation for sum-of-sinusoids

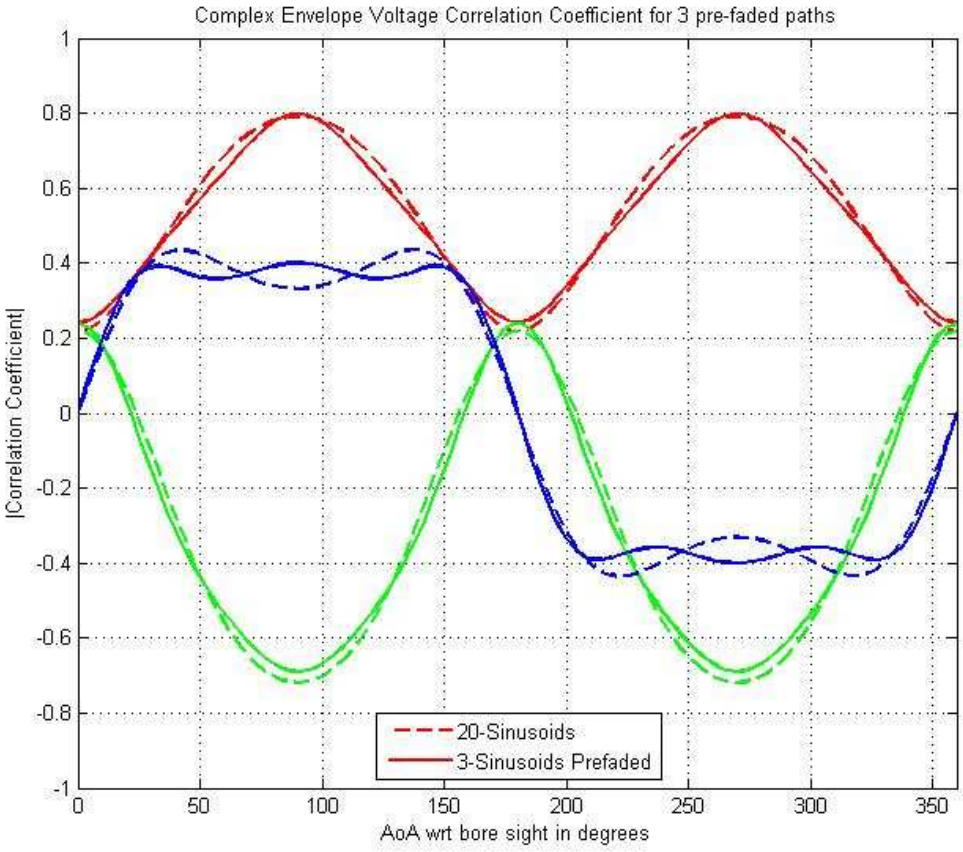

Figure 2.16 Spatial correlation using 3 pre-faded and power weighted signal paths

The spatial correlation using the three power weighted pre-faded (Rayleigh) components is shown in figure 2.16. It can be seen that the prefaded signal gives a very good approximation to the correlation obtained by using SCM (20-sub path) case.

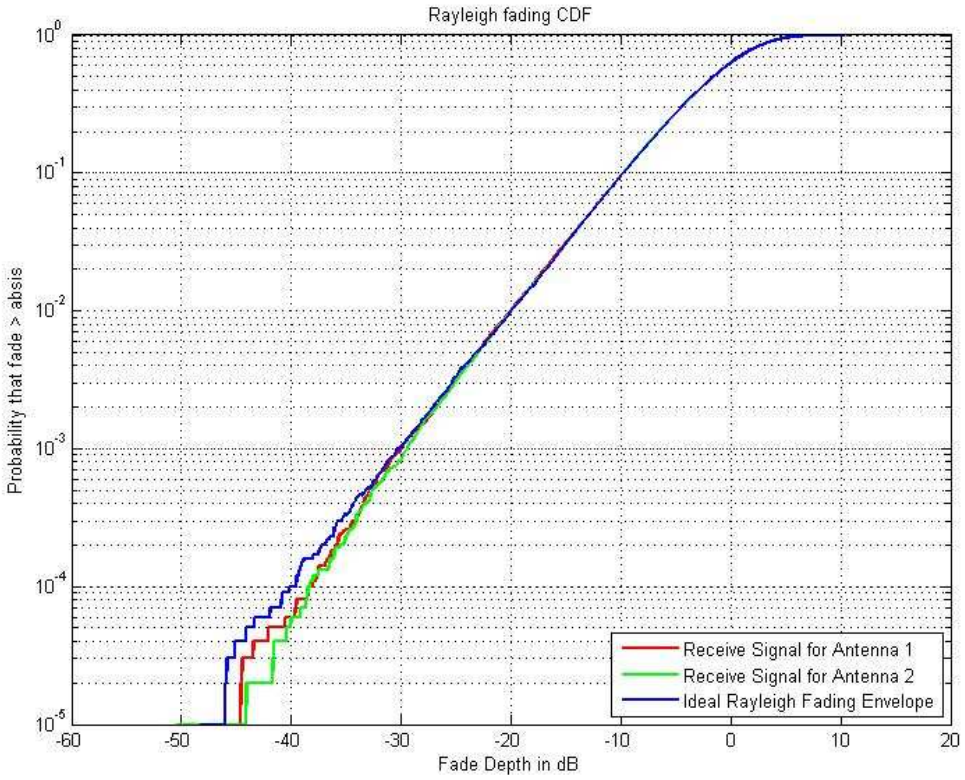

Figure 2.17 Pre-faded signal envelope CDF [20]

Figure 2.17 shows that if the small number of power weighted components are prefaded then they give rise to a matching behavior with the ideal case. It is observed [19] [20] that the autocorrelation function for this model follows the ideal autocorrelation function. Thus it is clear that by prefading the small number of signal components the *first-order* and *second-order* statistics of the multipath signal are preserved. This approach will be used to generate the test signal for OTA testing. More over the analysis shown in [18] [19] confirms that this model is antenna independent. That means a variety of possible antenna arrangements can be used and the antenna patterns can be applied separately to the predefined path gains to produce a complete end to end radio channel model for evaluation and OTA testing.

CHAPTER 3

MEASUREMENT SYSTEM FOR OTA TESTING

3.1 Measurement System and its Components

The main objective of the MIMO OTA testing technique in this work is to measure the spatial correlation between the antenna elements. Based on the analysis shown in chapter 2 it is clear that the spatial correlation measurements can distinguish between the 'good' and 'bad' MIMO terminals. The MIMO channel model should reflect the spatial structure of the channel, thus the spatial correlation measurements can validate the channel structure.

The system level representation of the measurement set-up used to evaluate the over-the-air testing technique is shown in figure 3.1. The main components of the measurement system are listed below:

1) Anechoic Chamber
2) Antenna System
3) RF Channel Emulator
4) System Instrumentation
5) Lab VIEW Programming for Automated Measurements

The fading signals are obtained from the Channel Emulators supplied by Spirent Communications. The RF source at the Vector Network Analyzer is used as the reference for the measurement. The source signal is divided into 4 signal paths by using 1:4 powers Splitter. Out of these 4-signal paths, 3-paths will go to the input of Channel Emulators and the remaining one will act as the reference for S-parameter measurements at the Vector Network Analyzer.

The three fading signals with predefined power weightings will be given to the three transmitting probe antennas sitting inside the Anechoic Chamber. Amplifiers are used in each path to boost the signal level. The two receivers are placed on the turn table with the help of a mount. The received signal is given to S-parameter test setup and the antenna pattern for the

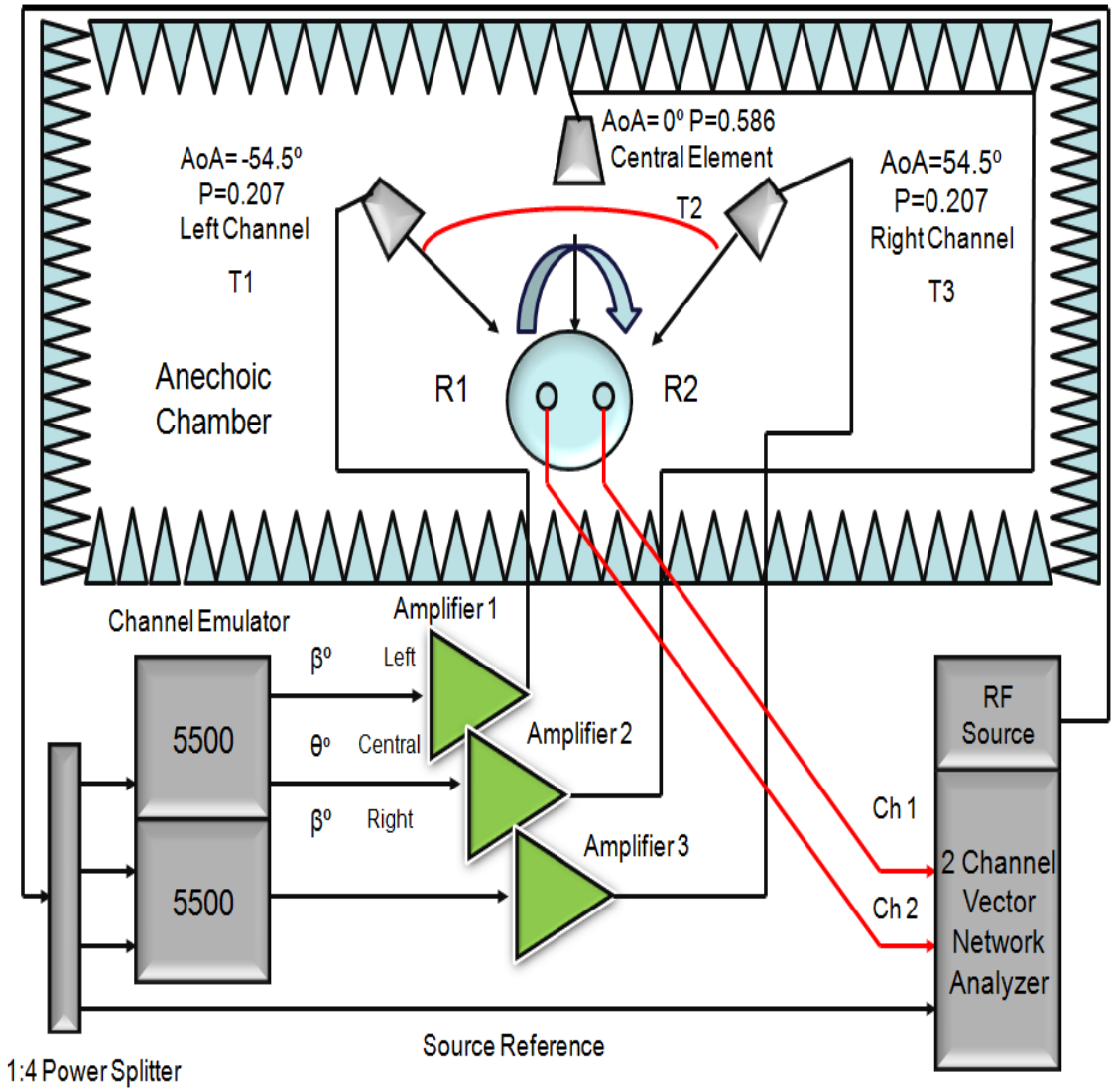

Figure 3.1 System level representation of the OTA test set-up

two probes is measured using VNA. The measurements are automated using the LabVIEW programming code. MATLAB routine is used for data processing and spatial correlation analysis. Following sections in this chapter will discuss each system component in detail.

3.1.1 Anechoic Chamber

The Anechoic Chambers are used to simulate the free space scenario inside the building. These chambers are developed to provide all weather capability and to minimize the electromagnetic interference observed in outdoor measurements. The walls of the chamber are covered with the RF absorbing materials in order provide good reflectivity performance. The physical dimensions of the RF absorbers will govern the quality of the reflectivity performance.

The design of the Anechoic Chamber is based on the geometrical optics techniques and each design attempts to reduce the specular reflections [26]. The Anechoic Chamber at UTA is designed in such a way that it is possible to carry out multi-static measurements. The chamber simulates the free space and maximizes the volume of available RF quiet zone.

Based on the specific geometries of the test probes a wide range of possible channels can be emulated and OTA testing can be carried out in the chamber. The spacing between the elements and the geometry involved in the probe positioning will be governed by the angle spreads being emulated in the test. Thus the channel model is a key factor in optimizing the chamber design for OTA testing [23]. The probes placed in the chamber may give some additional reflections of the signal. Thus, the mounting structure used to position the probes needs to be covered with RF absorbing material to minimize these signal reflections. The effect of signal reflections on the spatial correlation measurements are discussed in [23].

3.1.2 Antenna System

Two Sleeve Dipole probes are used at receiver and 3 horn antennas are used at transmitter to realize the MIMO link. Figure 3.2 shows the receiver array using two dipole elements. The decoupling sleeves are adjusted in length to get the desired impedance matching for each element. Dipoles are designed to use at the operating frequency of 1950 MHz. Figure 3.3 shows the probe positioning for the particular AoA. For spatial correlation measurements two sets of dipole antennas were used. One set had a pair of sleeve dipoles made in the lab,

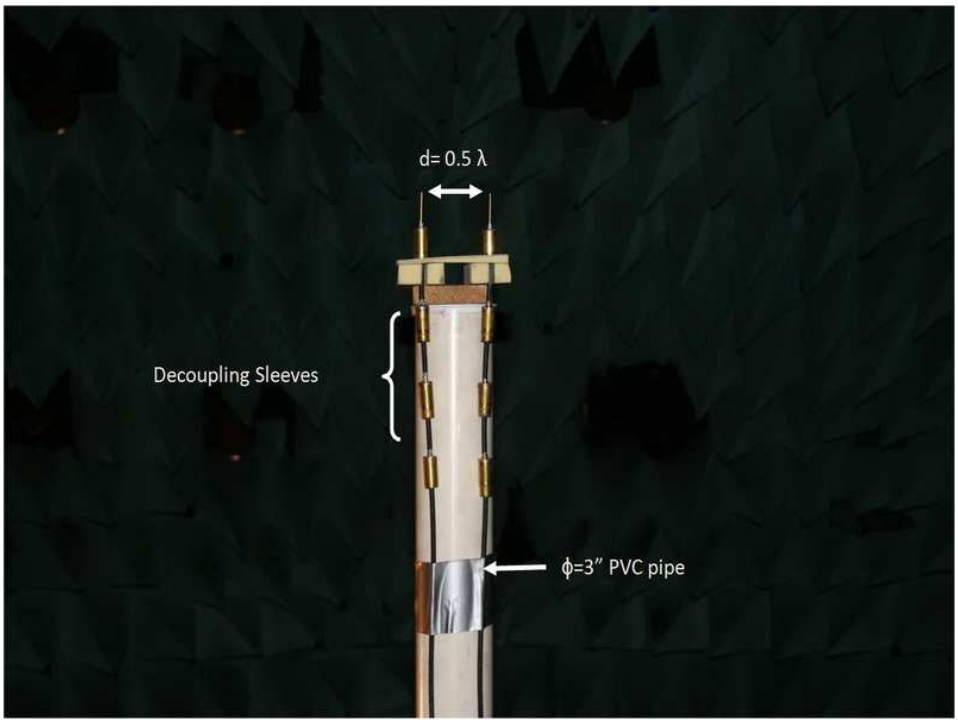

Figure 3.2 Two Sleeve Dipole Antennas at receiver

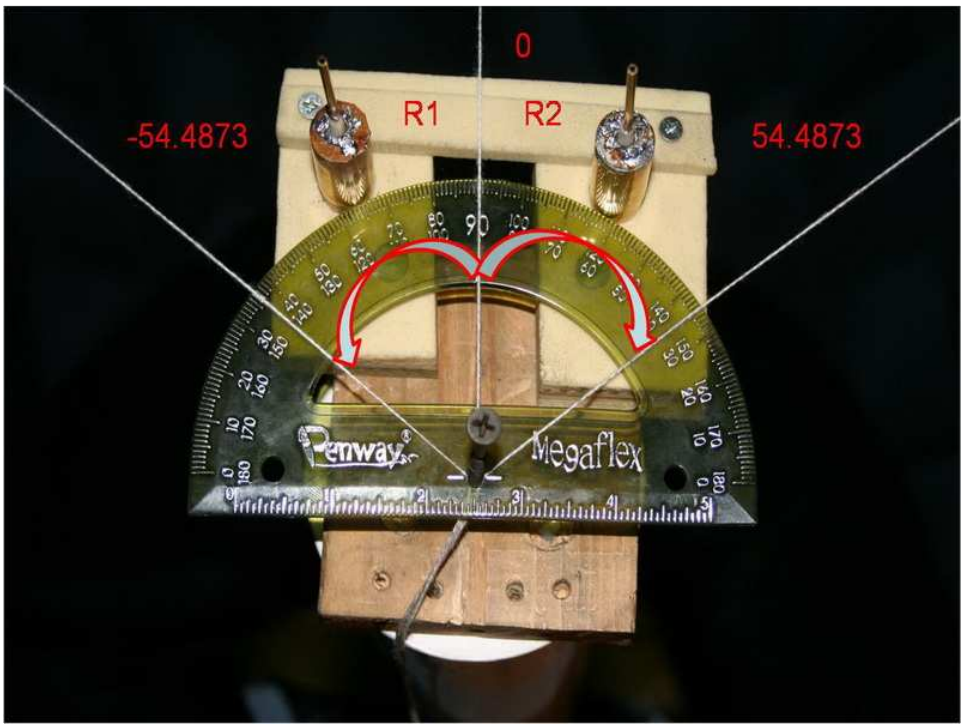

Figure 3.3 Angle of Arrivals for the Probes

which were tuned to 1950MHz. Each of the dipole had quarter wavelength long radiating element. The other pair had high precision dipole elements (AN303) which were designed to use for the frequency band of 1700 MHz to 2200 MHz. These dipoles were manufactured by BK precision.

The horn antennas are used as 3 transmitter probes. The angles of arrivals for the probes are defined with the reference of the array centre. T2 is the central element with AoA of 0^0. T1 and T3 are placed in the chamber with respect to this element. The probes are placed at same height as that of receiver to get MIMO radio link. By changing the elevation on each probe a Polarimetric dispersion can be obtained but this is not the intent of this set-up. A cluster is formed by placing the probe along the arc. The probe arrangement inside the chamber is shown in figure 3.4. The sleeve dipoles at the receiver are mounted on a 4'' PVC pipe. The fixture is placed on a (Azimuthal) turn table.

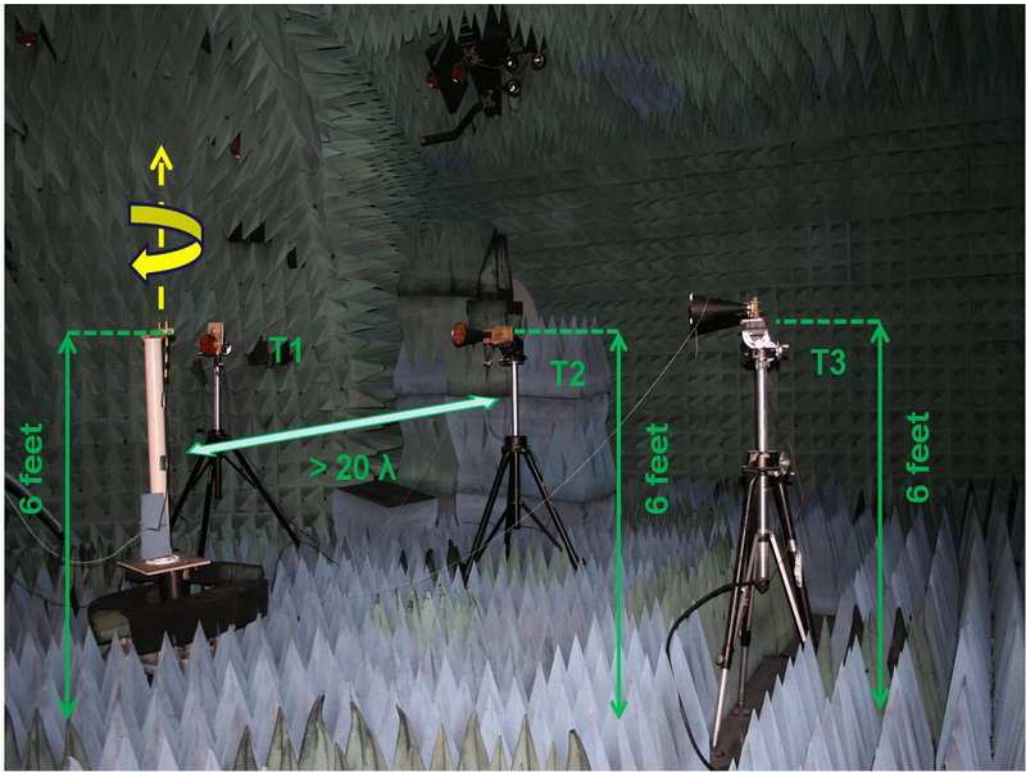

Figure 3.4 Probe set-up inside an Anechoic Chamber

3.1.3 RF Channel Emulator

MIMO RF channel is obtained by using two units of the RF Channel Emulators (SR 5500) supplied by Spirent Communications. The SR5500 emulates wideband radio channel characteristics such as time-varying multi-path delay spread, fast fading, shadow fading and channel loss for advanced receiver implementations using diversity, beamforming and MIMO.

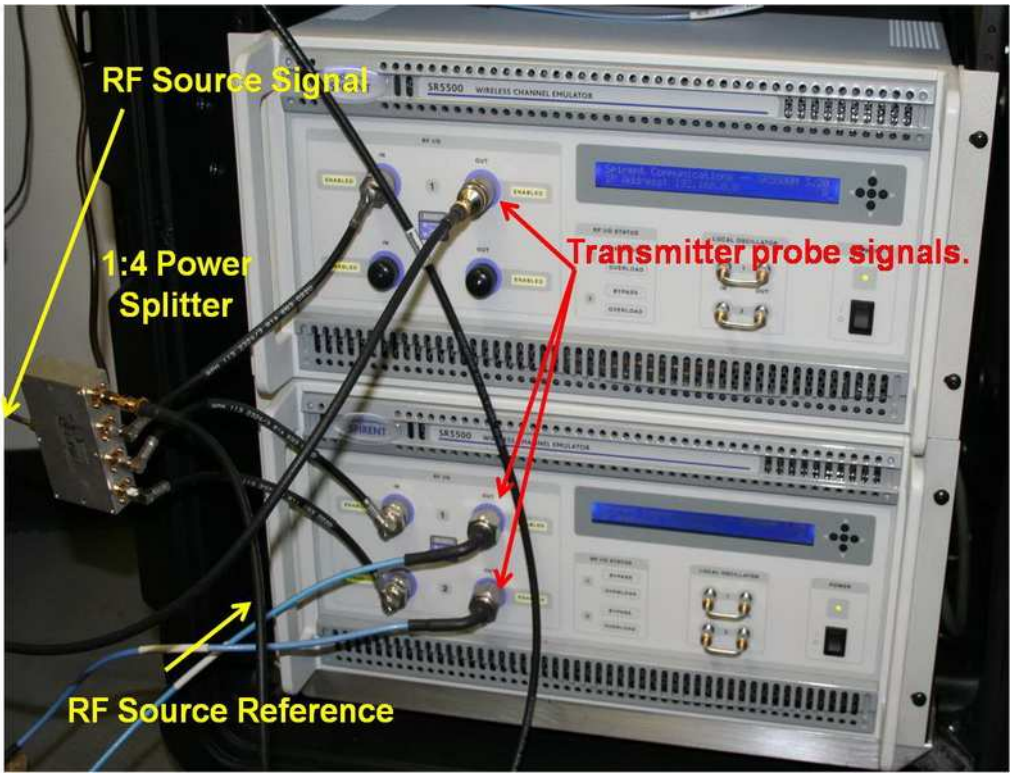

Figure 3.5 RF Channel Emulator

The set-up for the MIMO RF Channel Emulator is shown in figure 3.5. The RF signal from the synthesized sweeper is divided into the 4 signal paths out of which 3 signals are used as input to the 3 MIMO channels. The fourth signal from the splitter is used as RF reference in S-parameters measurements. Signal router is used to establish a communication link between two fader boxes and the PC.

The emulator has in-built digital RF power meter for each channel. This feature allows user to calibrate the individual channel power to the desired level. It is possible to generate a

fading window of particular length and this data can be stored and used again and again in play back mode. Each channel emulator can be used to realize a full 2x2 MIMO link.

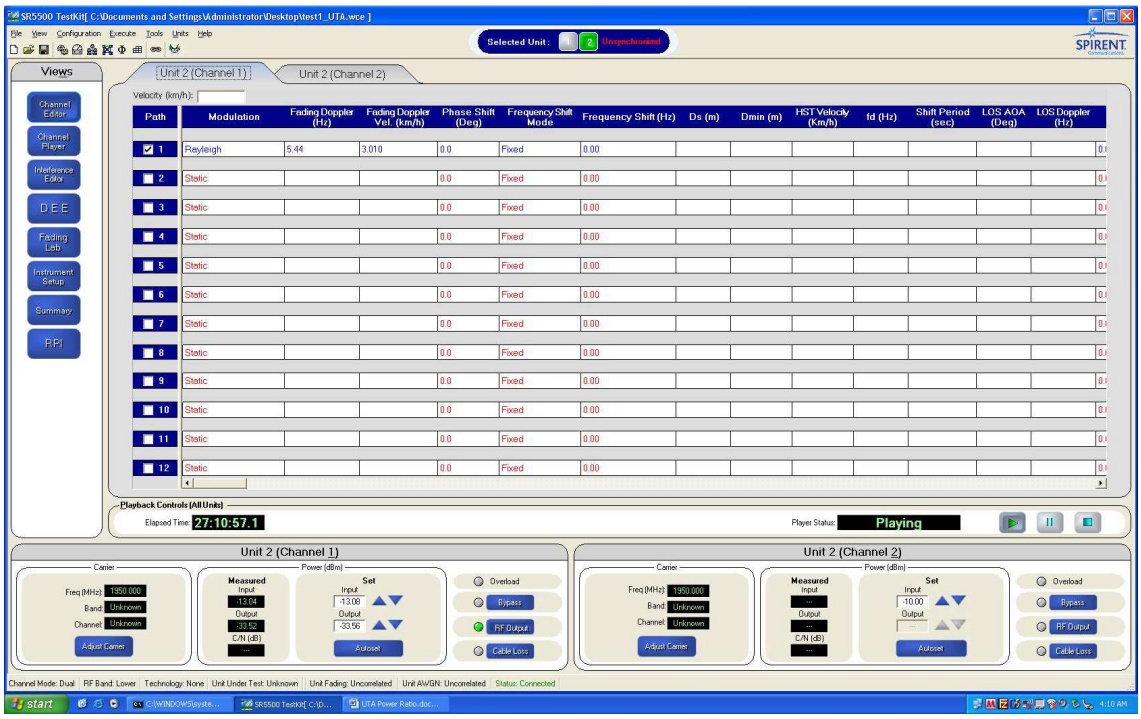

Figure 3.6 User Interface for RF Channel Emulator Boxes

The emulator replicates real-world spatial channel conditions, making it possible to isolate performance issues early in the development and design verification cycle. Additive White Gaussian Noise (AWGN) further enhances the real-world conditions emulated by the SR5500. Fader boxes can be used in Dynamic Environment Emulation mode or Fading Data Playback mode. The important technical specifications are listed in the Appendix section of this document. Figure 3.7 and 3.8 gives the Instrument set up view for the through configuration and the matrix configuration. The effect of path gains from each input and its dependency can be observed from these configurations.

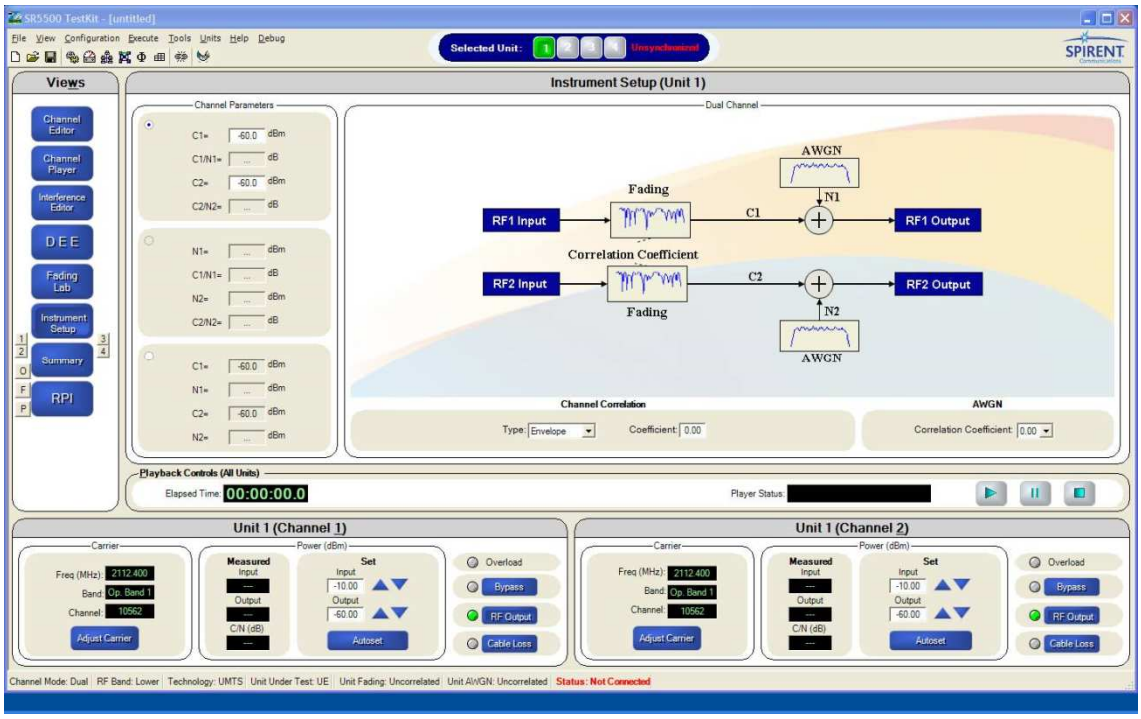

Figure 3.7 MIMO through configuration

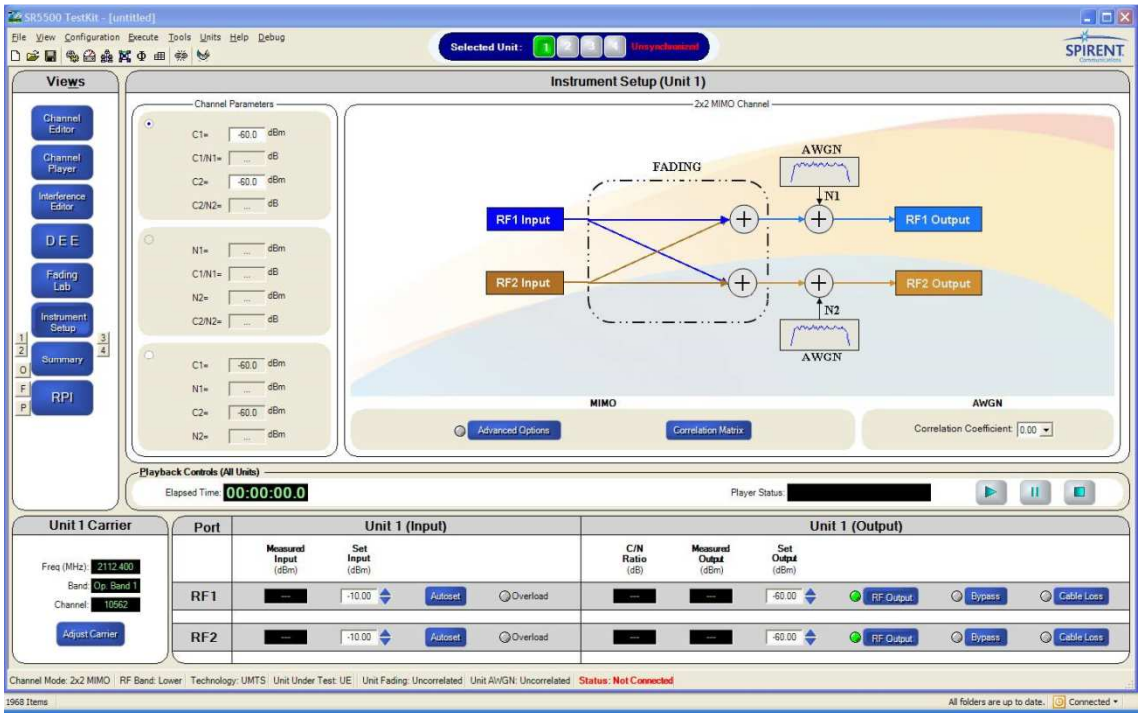

Figure 3.8 MIMO matrix configuration

The fader boxes basically generate the fading statistics either Rayleigh or Rician and uses a Doppler filter to get the wideband frequency selective channel behavior. For a random variable 'R ' the Rayleigh PDF is given by [30] (3.1),

$$p_R(r) = \frac{2r}{\Omega} e^{-r^2/\Omega}, \; r \geq 0 \tag{3.1}$$

Where $\Omega = E(R^2)$. The Rayleigh distribution can be obtained by using two zero-mean Gaussian random processes, which basically model the real and imaginary parts of the complex envelope observed in Rayleigh fading. The Doppler power spectral density of a fading channel describes how much spectral broadening it causes. For Rayleigh fading with a vertical receive antenna with equal sensitivity in all directions, this has been shown to be [30],

$$S(\nu) = \frac{1}{\pi f_d \sqrt{1 - \left(\frac{\nu}{f_d}\right)^2}} \tag{3.2}$$

Where, ν is the frequency shift relative to the carrier frequency. This equation is only valid for values of ν between $\pm f_d$; the spectrum is zero outside this range. This spectrum is shown in the figure 3.9 for a maximum Doppler shift of 10 Hz [30].

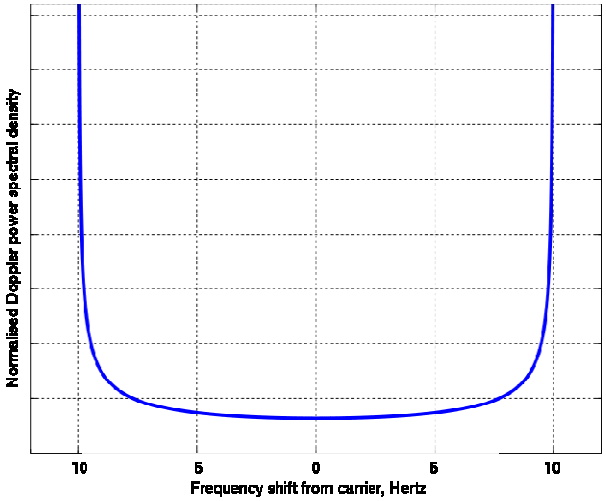

Figure 3.9 The normalized Doppler power spectrum of Rayleigh fading with a maximum Doppler shift of 10Hz [30]

The signal clusters observed in the multipath fading scenarios can be modeled by mean angel surrounded by an angular spread. Now this representation allows us to use the statistical PDF models to emulate the PAS of the received signal. PAS represents the average power as a function of angle.

In this work the geometry based spatial channel models are used to emulate MIMO channels observed in wideband cellular environment. The SCM and SCME uses the ray-based modeling technique which basically models each path by number of sub-paths as sum of sinusoids wherein each sinusoid represents the individual plane wave received by the antenna array at the receiver. Now the spatial correlation observed in these models is the effect of the narrow angular spread present in the channel.

The RF Channel Emulators generate the channel coefficients based on the specifications given in SCM and SCME standards to emulate MIMO channels. For an *S* element linear BS array and a *U* element linear MS array, the channel coefficients for one of *N* multipath components are given by a *U* -by- *S* matrix of complex amplitudes. The channel matrix for the *n*th multipath component (*n* = 1,…,*N*) is denoted as $\mathbf{H}_n(t)$. The (*u, s*)th component (*s* = 1,…,*S*; *u* = 1,…,*U*) of $\mathbf{H}_n(t)$ is given by [13],

$$h_{u,s,n}(t) = \sqrt{\frac{P_n \sigma_{SF}}{M}} \sum_{m=1}^{M} \begin{pmatrix} \sqrt{G_{BS}(\theta_{n,m,AoD})} \exp\left(j\left[kd_s \sin(\theta_{n,m,AoD}) + \Phi_{n,m}\right]\right) \times \\ \sqrt{G_{MS}(\theta_{n,m,AoA})} \exp\left(jkd_u \sin(\theta_{n,m,AoA})\right) \times \\ \exp\left(jk\|\mathbf{v}\|\cos(\theta_{n,m,AoA} - \theta_v)t\right) \end{pmatrix} \tag{3.3}$$

Where,

P_n is the power of the *n*th path.

σ_{SF} is the lognormal shadow fading , applied as a bulk parameter to the n paths for a given drop.

M is the number of sub paths per-path.

$\theta_{n,m,AoD}$ is the AoD for the mth Subpath of the nth path.

$\theta_{n,m,AoA}$ is the AoA for the mth Subpath of the nth path.

$G_{BS}(\theta_{n,m,AoD})$ is the BS antenna gain of each array element.

$G_{MS}(\theta_{n,m,AoA})$ is the MS antenna gain of each array element.

j is the square root of -1.

k is the wave number $2\pi/\lambda$ where λ is the carrier wavelength in meters.

d_s is the distance in meters from BS antenna element s from the reference (s = 1) antenna. For the reference antenna s = 1, d_1=0.

d_u is the distance in meters from MS antenna element u from the reference (u = 1) antenna. For the reference antenna u = 1, d_1=0.

$\Phi_{n,m}$ is the phase of the mth Subpath of the nth path.

$\|\mathbf{v}\|$ is the magnitude of the MS velocity vector.

θ_v is the angle of the MS velocity vector.

The path loss and the log normal shadowing is applied as bulk parameters to each of the sub-path components of the n path components of the channel [13].The MIMO capability of these emulator boxes is realized by these channel matrix coefficients.

For narrow angle spread signals the Doppler spectrum is different than the one shown in figure 3.9. The Doppler spectrum basically gives the temporal behavior of the combined plane wave signal received at antenna array. Now this includes the effect of angular spread (AS), AoA, DoT and the speed of the MS antenna. For the Laplacian distributed PAS of the signal the Doppler spectrum is given by [31],

$$S(f) = \frac{\sqrt{2}e^{-\frac{\sqrt{2}}{\sigma}\left|\cos^{-1}\left(\frac{f}{f_m}\right)-\mu\right|}}{f_m\sqrt{1-\left(\frac{f}{f_m}\right)^2}}$$

(3.4)

Where, $|f| \leq f_m$, and μ is the angle difference between the average AoA and the DoT, and f_m is the maximum Doppler frequency.

This Doppler spectrum mentioned in (3.4) is used to get the Doppler filter which defines the temporal behaviors observed in narrow angle spread signals. This approach is the new method by which the spatio-temporal dependency of the MIMO channel is realized. The RF Emulator defines the channel coefficients either by using (3.3) or by using (3.4). The filter-noise fader approach is discussed in [31]. The correlation based channel modeling uses (3.4) to filter the complex uncorrelated Gaussian i.i.d signals to get the faded temporal signal. This faded temporal signal is eventually used to represent the complete spatially and temporally correlated channel path between the multiple antennas [31].

3.1.4 System Instrumentation

3.1.4.1Vector Network Analyzer along with Synthesized Sweeper and Frequency Converter

The most important aspect of correlation measurement is that the data from both receivers needs to be measured simultaneously. In order to maintain the spatio-temporal characteristics of channel seen by both the probes the concurrent measurements are necessary.

In order to achieve this VNA is used in dual channel mode. However it is worth noting that the VNA uses frequency converter test set (S-parameter test set) to calculate the S-parameters. The S-parameter test set is fed with the two received signals from the receiver

array. The RF source of VNA is connected to the port 'a_1' of S-parameter test set with which acts as reference to all measurements. Channel Emulators also work on the same reference source in order to maintain the consistency of the test set-up. It is essential to check that the received signal is above the Noise floor of the VNA. The free space path loss and cable loss attenuates the transmitted signal with a magnitude of almost 50-60 dB until it reaches to the receiver array. VNA should be able to measure this low power signal. As the measurements are relative i.e. the ratios are calculated to get S-parameters, the reference on 'a_1' needs to be adjusted to a proper power level.

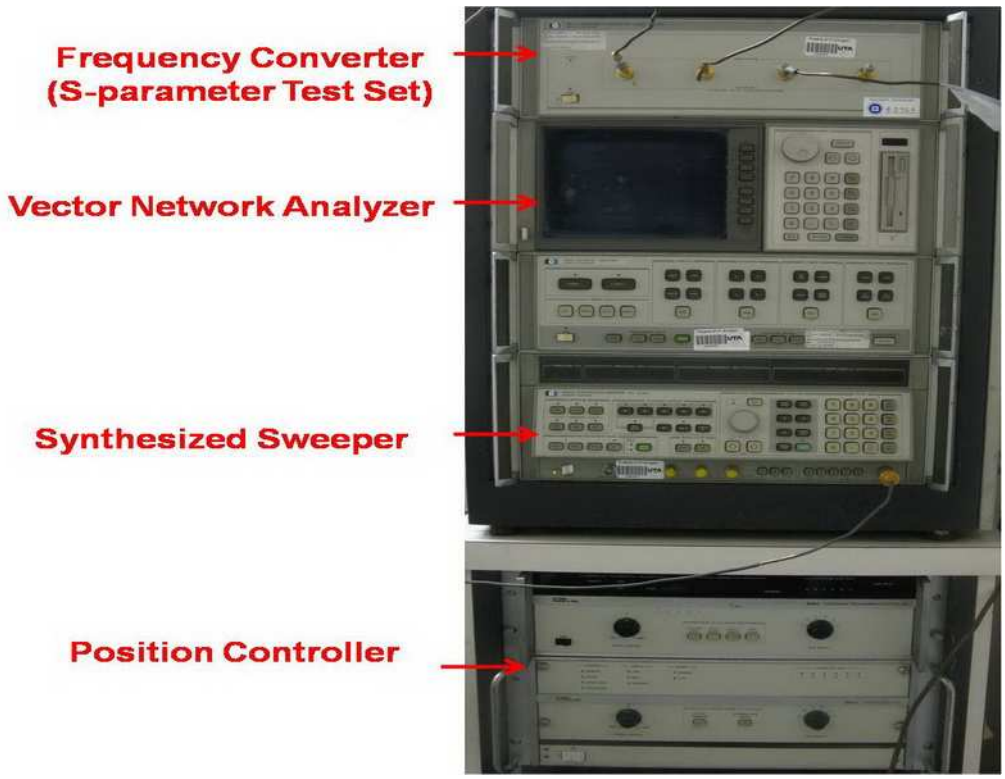

Figure 3.10 VNA set-up

The signal from receiver 1 is given to the 'b_1' input of the S-parameter test set and the signal from receiver 2 is given to the 'b_2' input of the S-parameter test set.

Thus, the S-Parameter test set measures the receive signal from probe 1 on the channel 1 as S_{11} and the signal from probe 2 on channel 2 as S_{21}. The VNA set-up is shown in figure 3.10.

3.1.4.2 Other System Components

In order to boost the signal coming from the channel emulator boxes, RF amplifiers are used on each of the 3 transmitting channels. 1:4 power splitter uses the same RF reference as that of VNA to generate 4 outputs out of which three are used as input to drive the fader boxes.

Semi-rigid cables are used for most of the part of the system to carry the signals. Gore cables are used at the receiver on one of the probe due to their high precision performance.

3.1.5 Lab VIEW Programming for Automated Measurements

National Instrument's Lab VIEW program is used to control all the measuring instruments. Lab VIEW program uses General Purpose Interface Bus (GPIB) to communicate with the instruments. GPIB is a standard interface for communication between instrument and controllers from various vendors. LabVIEW programs/subroutines are called virtual instruments (VIs). Each VI has three components: a block diagram, a front panel, and a connector panel. Figure 3.11 shows the front panel of the Lab VIEW VI used in this work. The front panel serves as a programmatic interface and it defines the inputs and outputs for the given node through the connector pane. A virtual instrument can either be run as a program, with the front panel serving as a user interface or, when dropped as a node onto the block diagram.

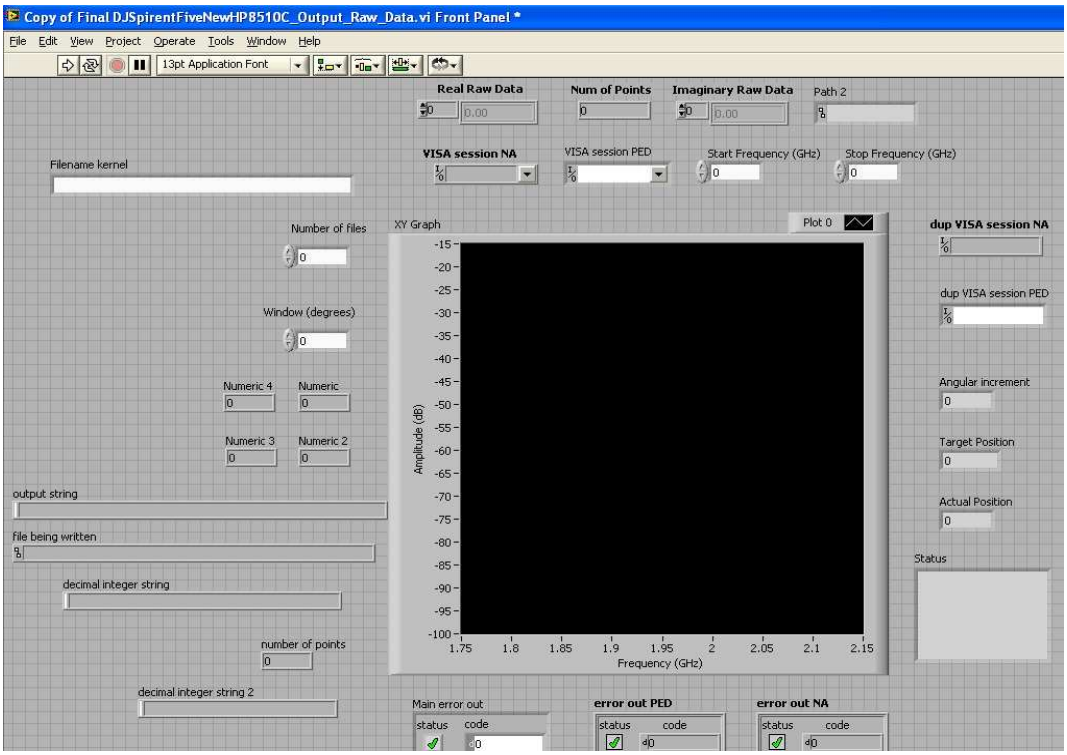

Figure 3.11 Front Panel Interface for Lab VIEW code

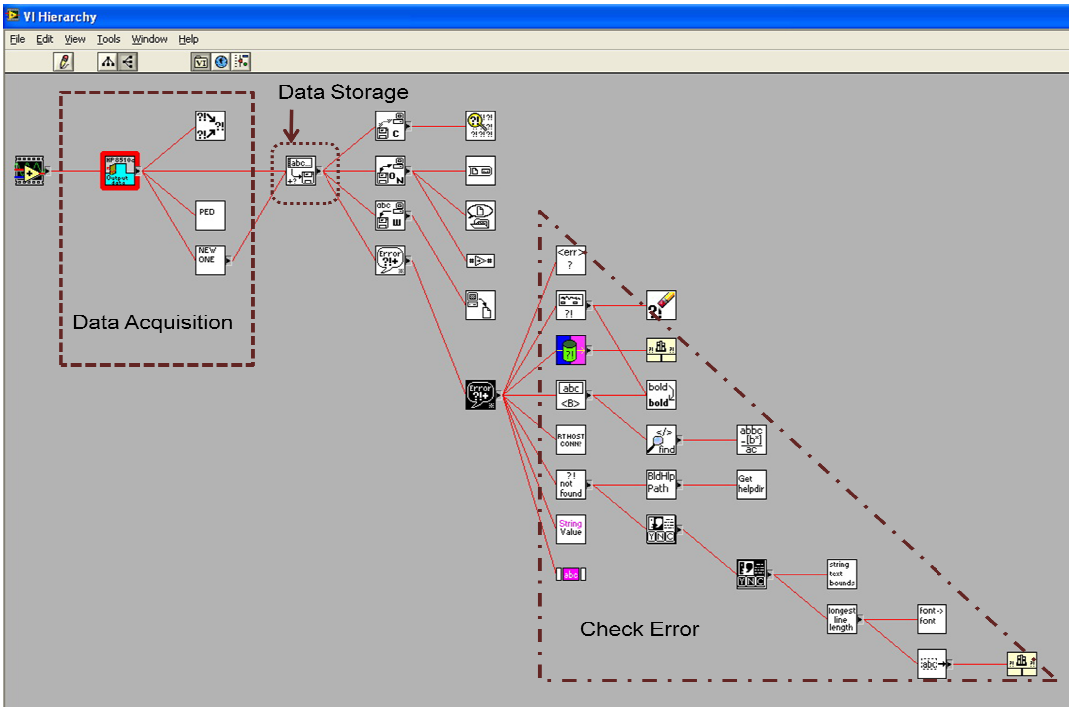

Figure 3.12 VI's Hierarchical structure

The Hierarchical structure of the VI used in this work is shown in figure 3.12. It has 3 main parts: Data Acquisition, Data Storage and Check Error Signal.

For correlation measurements it's essential that the system should be taking concurrent measurements at both receivers. The VI's available to control the system instruments could only measure the data on single receiver. The challenge was to take simultaneous measurements on each channel of the VNA. For simultaneous data logging the VNA is used in coupled channel mode. Based on the building blocks of the available VI a new sub-routine is developed which will do a single sweep on each channel (at the same instance) and then it will log the data in two different files. In order to collect enough number of samples to get good fading statistics the time evolved sequence is measured multiple times at the predefined angular positions.

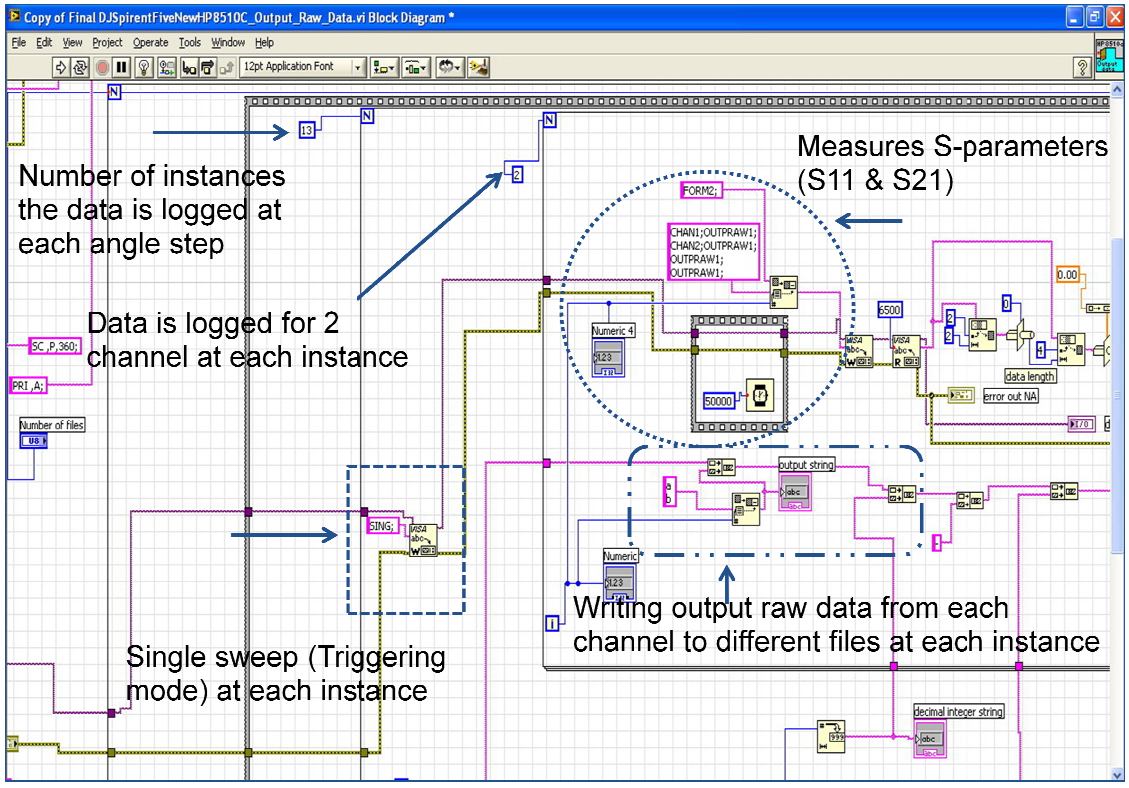

Figure 3.13 Partial View of the Block Diagram for new VI

The partial view of the block diagram for new VI can be seen in figure 3.13. In order to collect more than 801 data points at a particular angular position a 'for loop' is added. The index

on this for loop needs to be edited as per the required number of sample points. For example if we need 10K samples at each angular position then the indexing number will be 10K/801 which is 13. At each instance the VNA should trigger only once so that the data will be held until it is written into the file specified by the user. Thus the time coherent measurements are carried out. The S-parameter test set measures the signal on the each channel and the output of the test set is in the form of the RAW data (complex voltages). Thus, for a particular position the data will be measured and stored for index number of times. Once the indexing is over the sequential frame will execute the X-Y plot routine and will run the Pedestal control VI. This sequence will follow until the Pedestal moves through the number of angular steps mentioned by the user at the front panel.

CHAPTER 4

EXPERIMENTAL RESULTS AND ANALYSIS

4.1 MIMO OTA Testing

The MIMO OTA testing was carried out in two steps: Initializing the system parameters for Radiation pattern measurements using two antenna elements and spatial correlation measurements for 3-component model. The test plan for the same is described below,

Phase 1:

1. Configure the VNA for coupled channel mode with continuous wave (single frequency) triggering method. Set maximum number of points per sweep. Select S_{11} and S_{21} on channel 1 and channel2 respectively.
2. Configure the Lab VIEW code to collect radiation pattern data for each angular position with the resolution of 5^0.
3. Start the measurements and collect the radiation pattern characteristics for two sets of dipole elements.

Phase 2:

1. Initialize the RF channel emulator boxes and establish a communication link between the PC and the fader units.
2. Replace the dipole array fixture at the receiver by a horn antenna in order to carry out power calibration for each transmitter channel
3. Activate each channel from the RF channel emulator units at a time and calibrate power on each of them by pointing the horn in the direction of the active channel. Start with central element, deactivate the other 2 outputs of the

units and then calibrate the RF output power so that the central unit will have 58.60% of the total power as compared to the other two channels.

4. Point the horn to the other channel, activate that particular output of the channel emulator unit and then calibrate the power at the emulator units so as to get the 20.7% of the total power for this channel.
5. Repeat step 4 for the remaining third transmitter and calibrate it to transmit remaining 20.7% of the total power.
6. This calibration is most critical in achieving proper spatial correlation values. This procedure takes care of the total link power budget which includes losses accounting for cables (at transmitters) + free space + cables (at receiver).
7. All the horns used at transmitter and at the receiver are of the same make. The set up for the power calibration is shown in the figure 4.1.

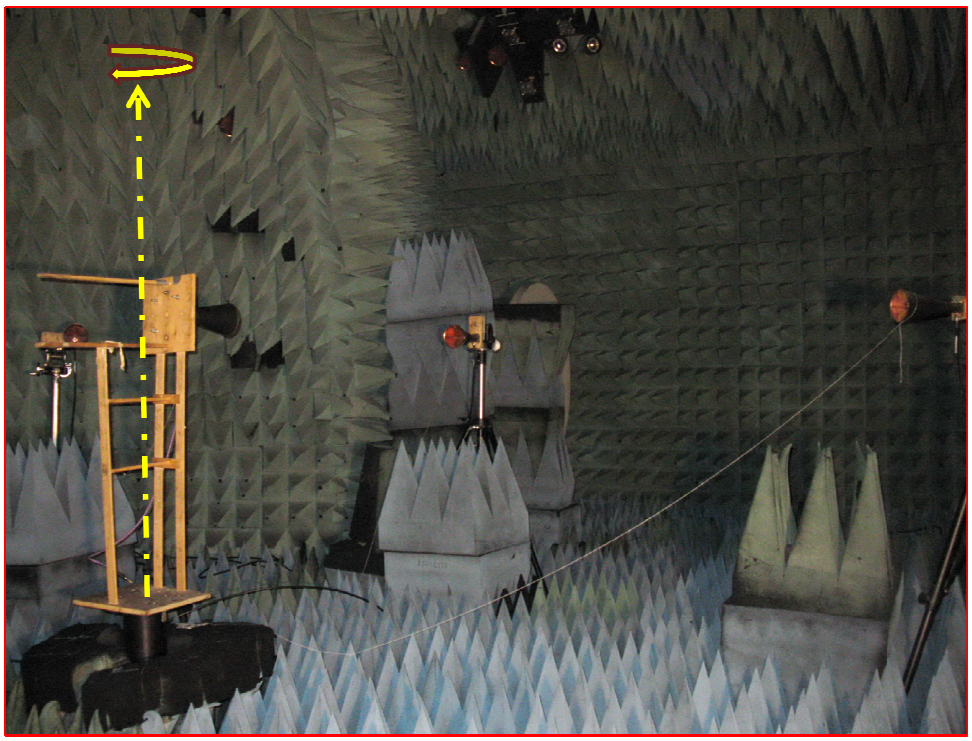

Figure 4.1 Set-up for Power Calibration

8. After power calibration, replace the receiver fixture with the dipole array and then configure the RF channel emulator for generating the Rayleigh fading signals on the each channel. Each channel was given different Doppler velocity so that the fading sequence from each channel will be uncorrelated as much as possible.
9. Set the Lab VIEW input parameters to collect 10 K samples at each angular position. Take the readings for each 10^{0} steps.

4.2 Results and Analysis

4.2.1 Antenna Pattern measurements

As discussed earlier the radiation pattern measurements were carried out. It is necessary for the OTA test system to provide repeatability of the measurements. The measurements were carried out for three independent sets of readings. The voltage gain plots for these sets are shown in figure 4.2, 4.3 and 4.4.

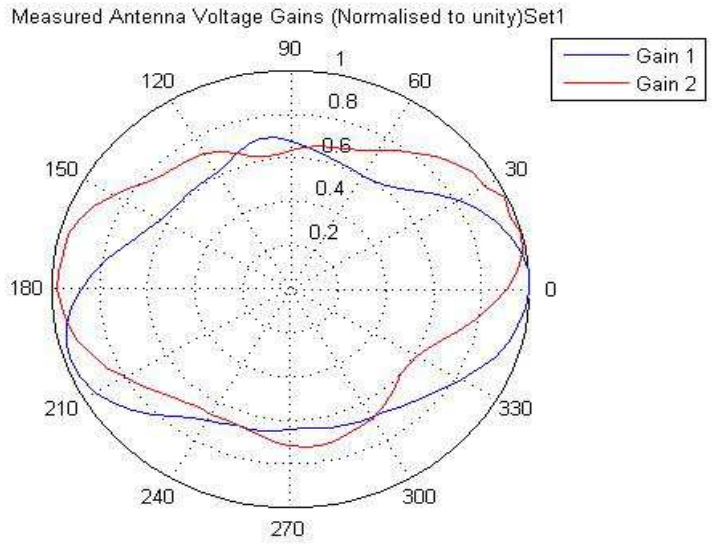

Figure 4.2 Measured Antenna Voltage Gains Set-1

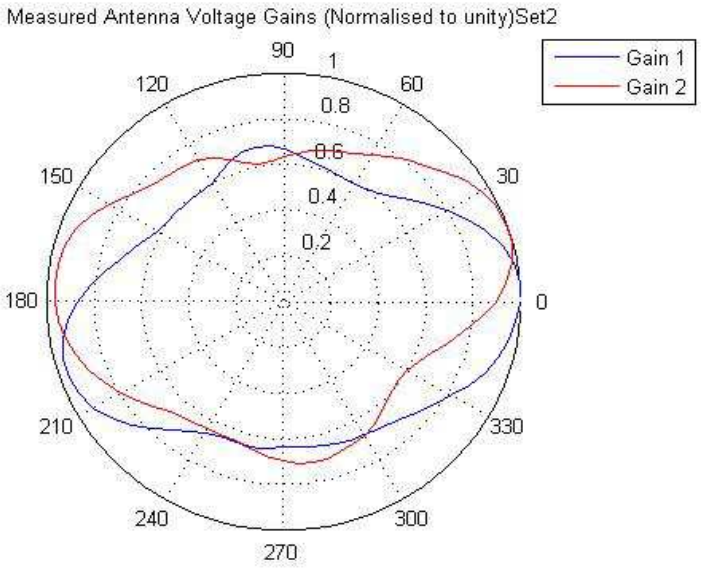

Figure 4.3 Measured Antenna Voltage Gains Set-2

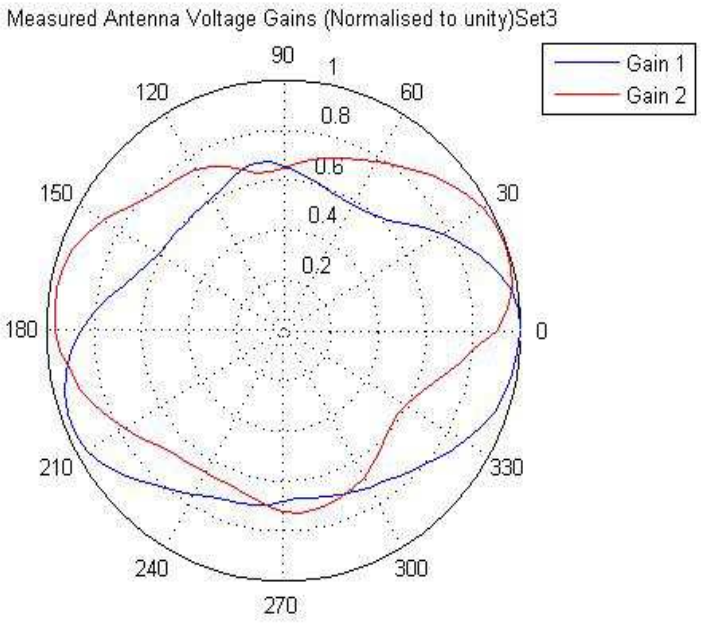

Figure 4.4 Measured Antenna Voltage Gains Set-3

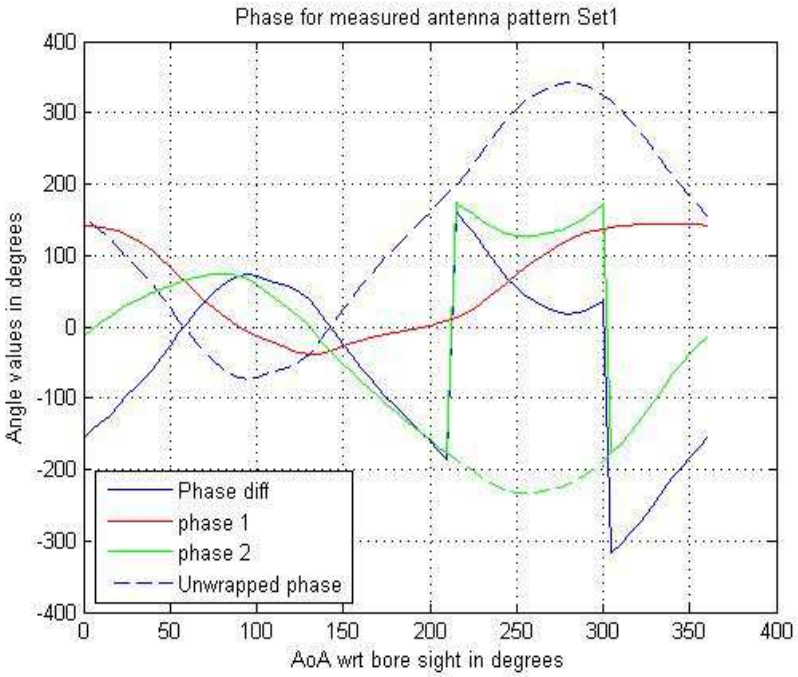

Figure 4.5 Measured Antenna Phase Response Set-1

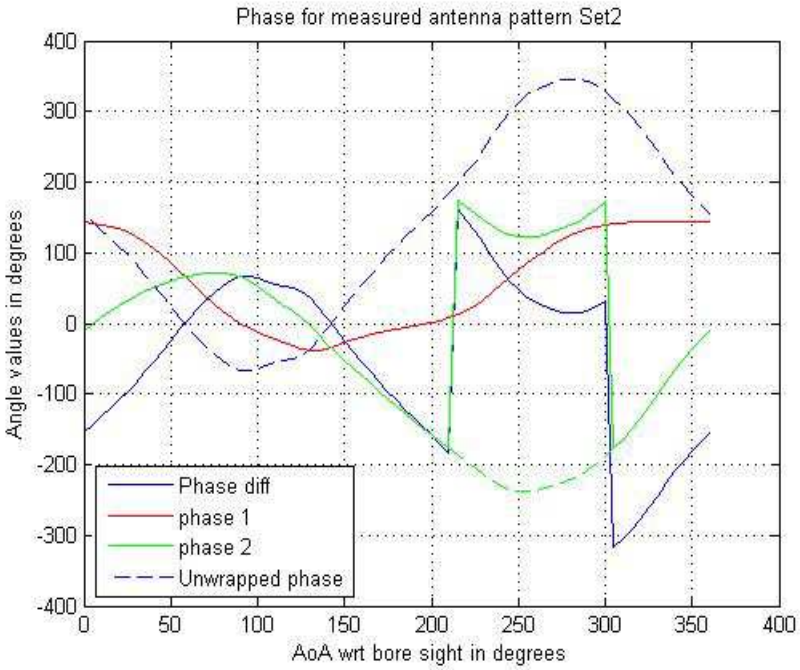

Figure 4.6 Measured Antenna Phase Response Set-2

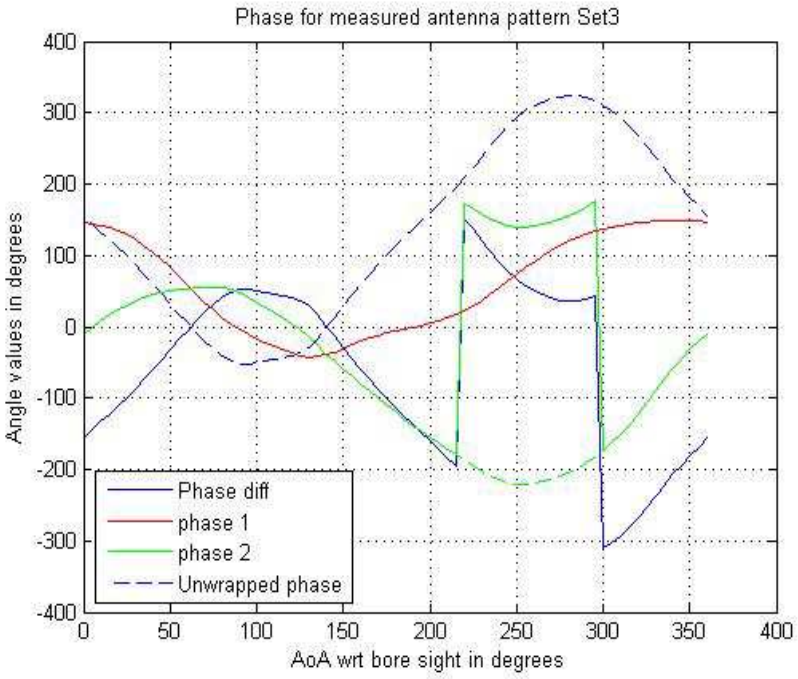

Figure 4.7 Measured Antenna Phase Response Set-3

The phase response for the same set of readings is plotted using the MATLAB routine. These phase responses are shown in figure 4.5, 4.6 and 4.7. It can be observed clearly that the system performance is repeatable to greater degree.

4.2.2 Prediction of Complex Envelope Voltage Correlation Coefficients using the Antenna pattern set-1

The normalized voltage gain values and the phase values from set 1 are used to predict the complex voltage correlation coefficients for the 3-component model. These predicted plots are shown in figure 4.8. The effect of normalization on the spatial correlation measurement is observed in these plots. Two-way normalization is used, in first approach the voltage gains are normalized to unit voltage and then these values are used to predict the spatial correlation values. The magnitude for the predicted complex voltage correlation is shown by the dashed redlines. Another approach is that the magnitudes are normalized to unity power level and then those values are used for correlation measurements. These values are shown by the solid red line.

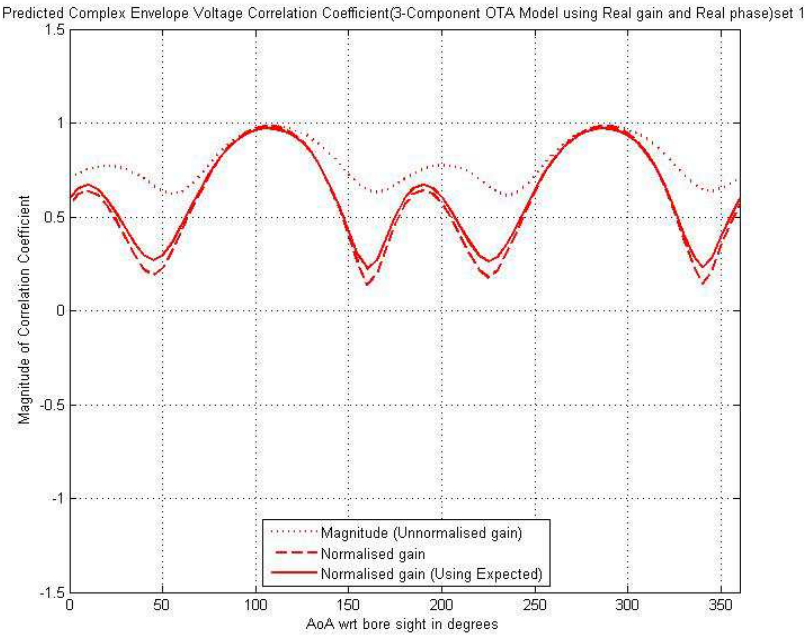

Figure 4.8 Predicted values for Spatial Correlation Measurements (Effect of Normalization)

4.2.3 OTA measurements for MIMO channel

4.2.3.1. Antenna Pattern Measurements using Sleeve Dipoles

The sleeve dipoles with the decoupling sleeves on them were used for the first set of 3x2 MIMO channel. The antenna gain voltage plots are shown in figure 4.9. The *first-order* statistics of the MIMO channel are obtained and they are shown in figure 4.10. The fading statistics follow the ideal Rayleigh fading CDF.

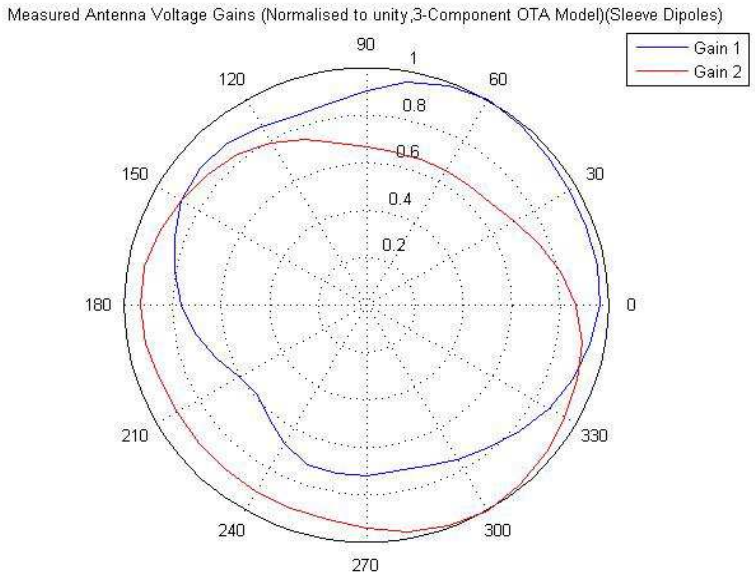

Figure 4.9 Measured Antenna Gain responses for 3-Component model using Sleeve Dipoles

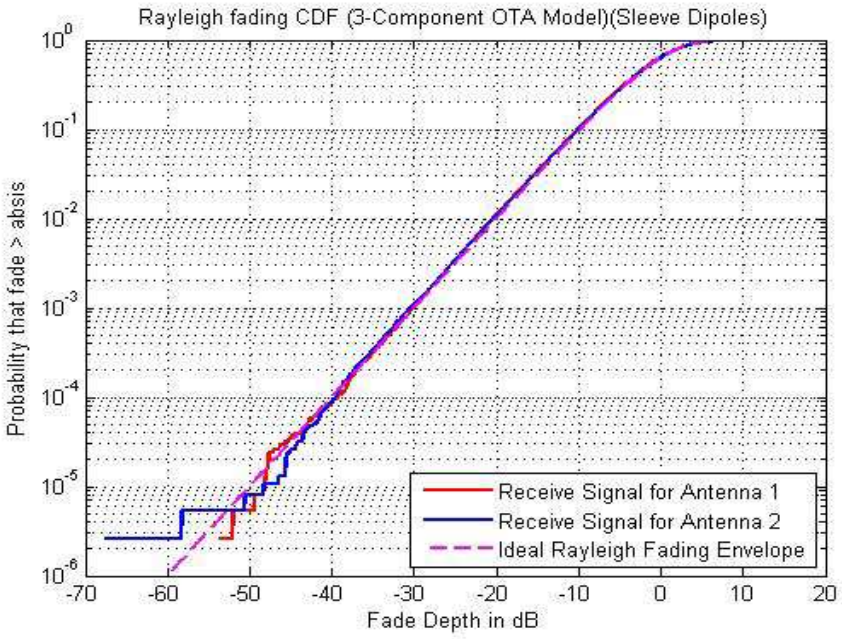

Figure 4.10 CDF for the fading signal using Sleeve Dipoles for 3-Component model

4.2.3.2. Measured Complex Envelope Voltage Correlation Coefficient using Sleeve Dipoles

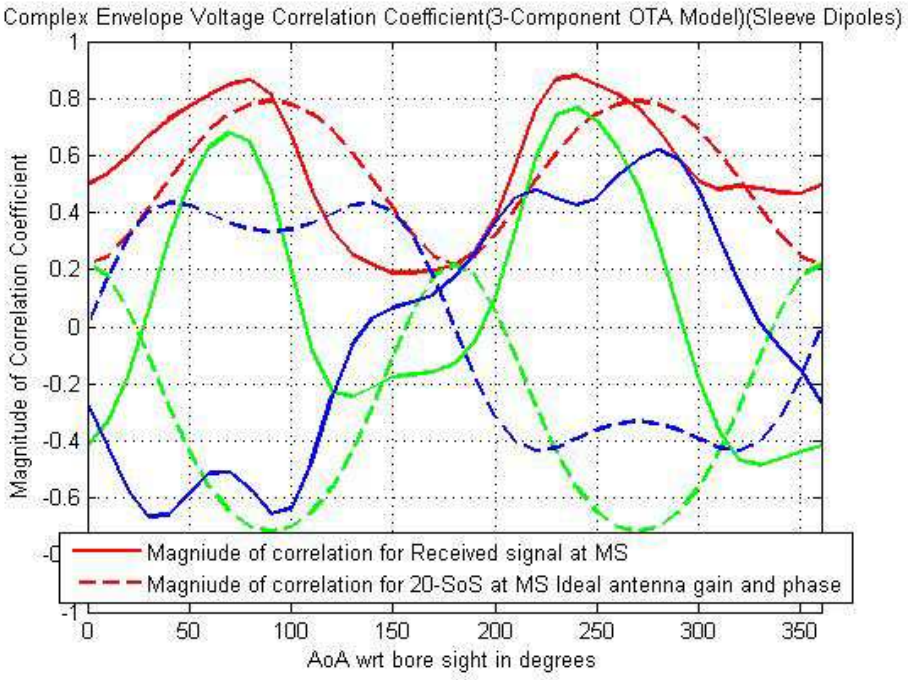

Figure 4.11 Measured Spatial Correlation for the 3-Components using Sleeve Dipoles

Figure 4.11 shows the measured values for complex envelope voltage correlation coefficients. I and Q values for the same are also plotted in the figure. The solid red line represents the magnitude of the measured complex correlation coefficients wherein the dashed red line represents the magnitude of the ideal case (20-sub paths, uncoupled Omni case). It can be observed that the magnitude levels are preserved in this measured data they match well to the expected values. It looks like that the measured curve is falling behind the ideal data, this is due to the phase offset present at the antenna elements due to different cable lengths and the offset of DUT on the turn table. This will be explained later in detail at the end of this chapter. For these measurements the Fading Data Playback mode was used on the RF channel emulator units.

4.2.3.3. Antenna Pattern Measurements using Precision Dipoles

The next set of measurements for spatial correlation was carried out using the high precision dipoles manufactured by BK Precision. The measured voltage gains are shown in figure 4.12.

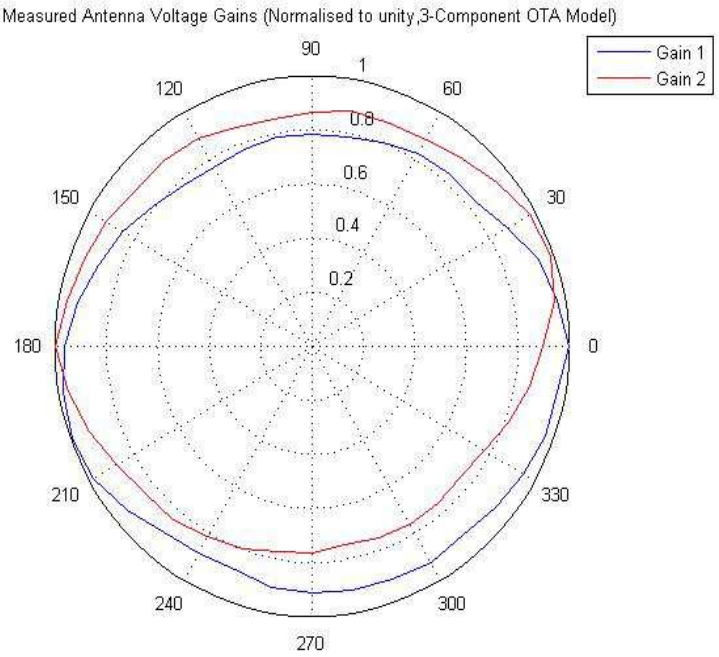

Figure 4.12 Measured Antenna Gain responses for 3-Component model using Precision Dipoles

The *first-order* statistics of the received signals are shown in figure 4.13. These CDF values are compared with the ideal Rayleigh fading CDF. They show almost no deviation from the ideal curves for the fade depth up to -40dB. Figure 4.14 gives a snapshot of the Time evolved fading signal observed at the receiver.

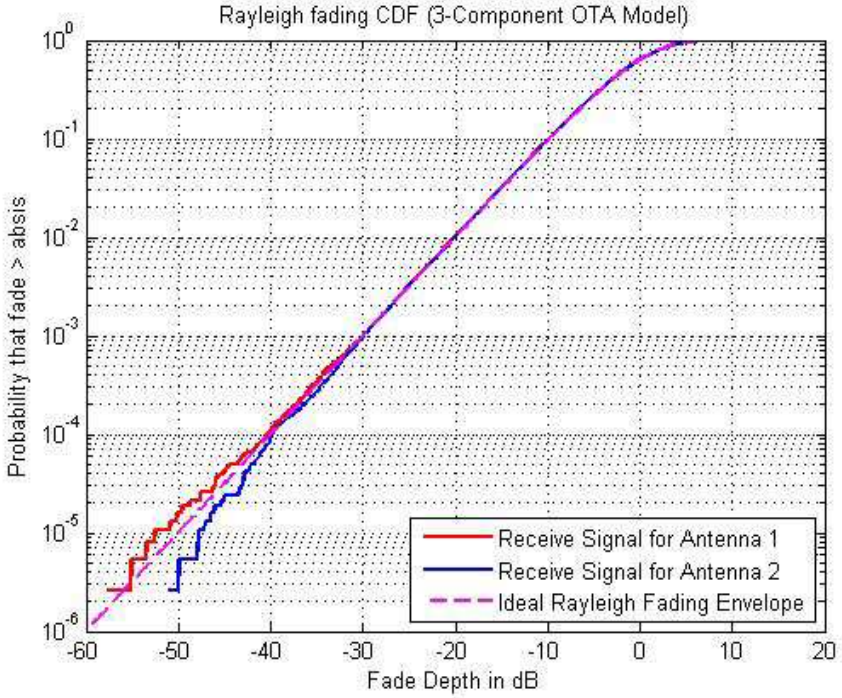

Figure 4.13 CDF for the fading signal using Sleeve Dipoles for 3-Component model

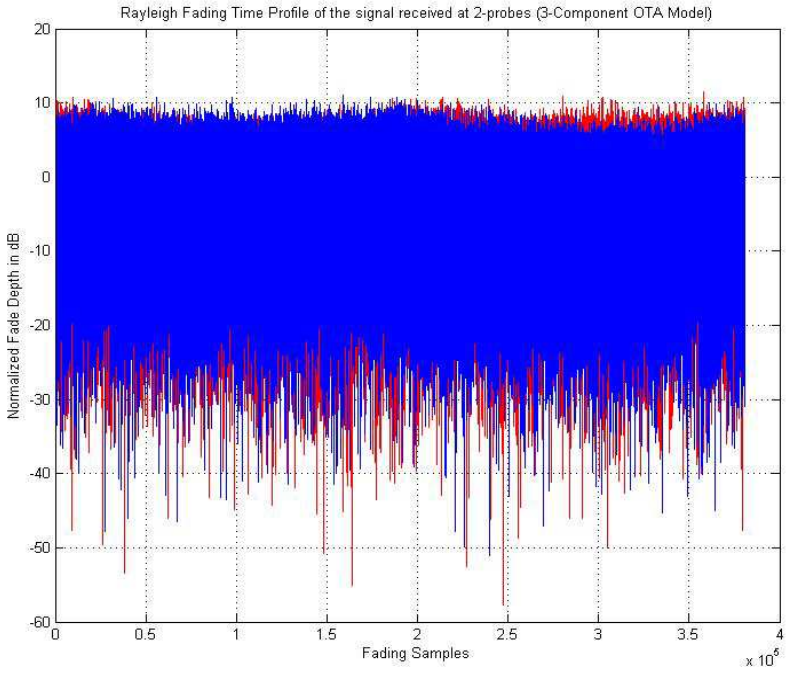

Figure 4.14 Time evolved fading signal at the receiver array

4.2.3.4. Measured Complex Envelope Voltage Correlation Coefficient using Precision Dipoles set-1

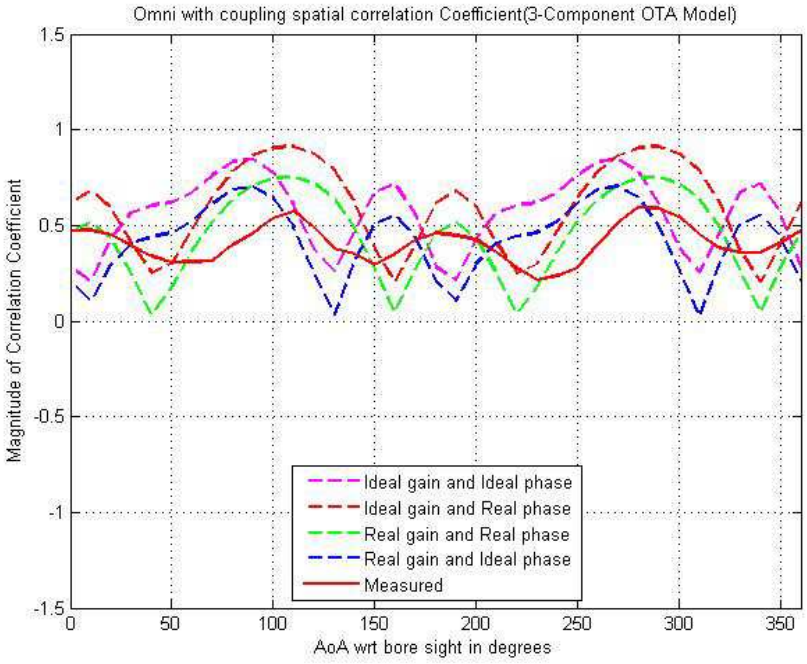

Figure 4.15 Measured Vs Predicted Spatial Correlation for Precision Dipoles using 3-Component Model (Coupled Omni case)

The measured complex envelope spatial correlation coefficients are shown by solid red line in the figure 4.15. These values are compared with respect to the different sets of predicted curves. These predicted curves uses the Ideal Gain values and Ideal phase values obtained from a method of moments (MOM) solver for omni coupled array response. The real gain and real phase mentioned over here are nothing but the measured antenna gain and phase response values at the particular AoA. The measured values seemed to be off from the expected values by a good amount. The best close match for the measured value was obtained by the dashed green line which uses the real gain and phase from the antenna response to predict the correlation coefficients. This mismatch was due to the mismatch observed in the power ratio on each channel, which is explained in figure 4.16.

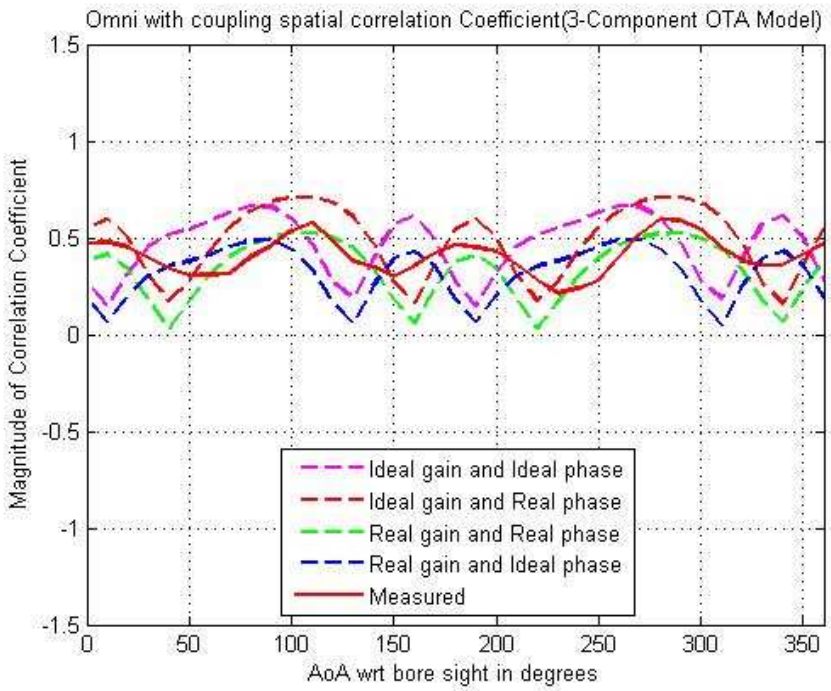

Figure 4.16 Measured Vs Predicted Spatial Correlation for Precision Dipoles using 3-Component Model (Drooping power case)

The same data set is processed with different approach in which it was assumed that the power ratio on the transmitter antenna was not maintained as per the 3- component model.

The central element in this case assumed to have 78.6% of the total power and the each of the other two elements had the 10.7% of the total transmitter power. By this assumption the values for spatial correlation were predicted. The dashed green line gives a substantial match to the measure data. It used real antenna phase and real antenna gains to predict the measured correlation values. Some of the mismatch seen in the measured data with respect to the predicted data is due to the phase variation encountered by the cable offset and turntable offset for DUT positioning.

4.2.3.5. Measured Complex Envelope Voltage Correlation Coefficient using Precision Dipoles Set-2

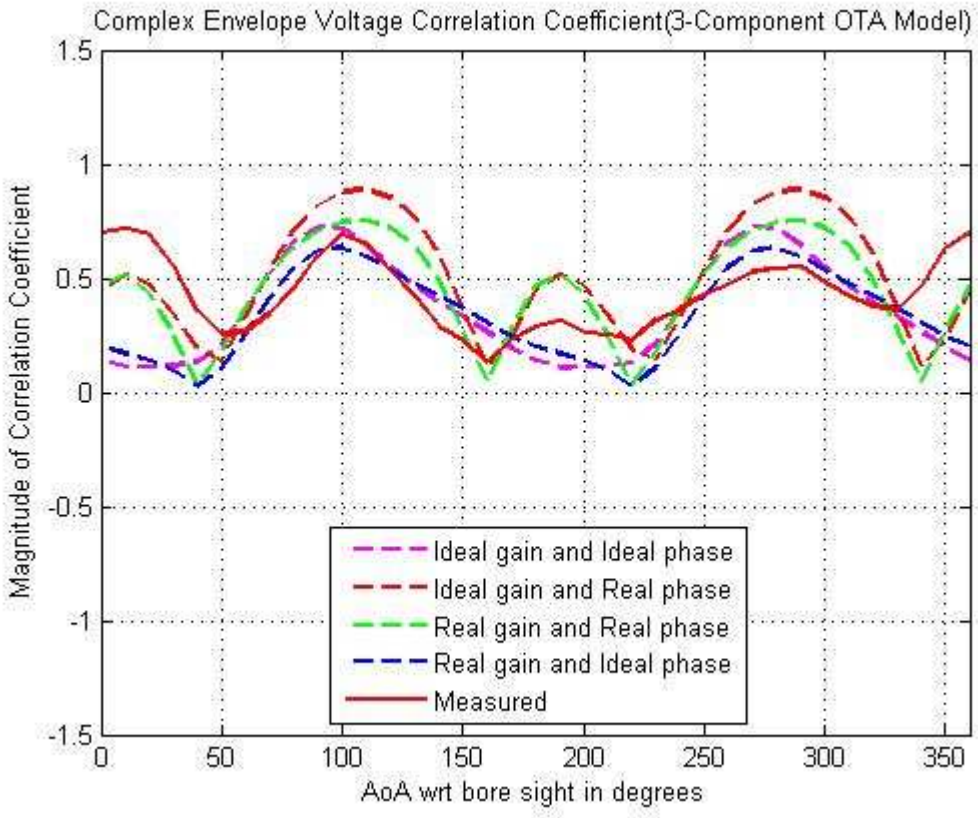

Figure 4.17 Measured Vs Predicted Spatial Correlation for Precision Dipoles using 3-Component Model Set-2 (Uncoupled Dipole elements case)

In order take out the effect of the drooping power, the power calibration for each link is performed again and a new set of measurements is obtained. This set gives good agreement on the minimum and maximum values for the predicted correlation coefficients. The predicted values shown in figure 4.17 are obtained by using the Ideal uncoupled omni data and the Ideal AoA for each transmitter antenna. A close match is obtained by using the real gain and real phase information. The same measured result is compared with the spatial correlation coefficients predicted using the coupled Omni case. The gain and phase response for the ideal coupled Omni case is obtained by using the MOM solver which was supplied by Spirent Communications. Those plots are shown in figure 4.18.

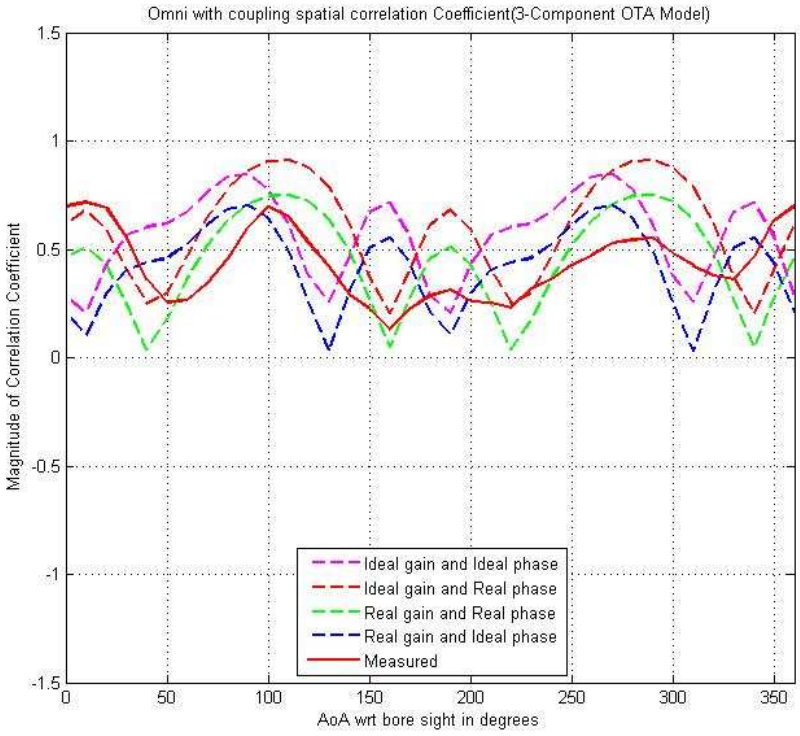

Figure 4.18 Measured Vs Predicted Spatial Correlation for Precision Dipoles using 3-Component Model Set-2 (Coupled Omni case)

Predicted values using the real gain and real phase along with the real gain and ideal phase gives a most close match to the measured data. The significant improvement to the dataset is obtained by properly calibrating the power level on each transmitting channels.

4.2.3.6. Offset Errors in phase measurements

The misalignment of the predicted data with the measured data was mainly due to the offset errors observed in the phase measurements. These offset errors origin from the different length of the cables at the receiver elements and the Design Under Test (DUT) offset on the turntable. This is explained in detail in figure 4.19. If the centre of the array is not on the axis of rotation of the array, then you can clearly see that, one antenna element will take a longer circumference path from the centre as compared to the other element. This positioning error in the fixture will affect the phase response of the array. When one element is gaining phase then

the other will lose phase more rapidly than expected, thus by giving rise to erroneous phase response.

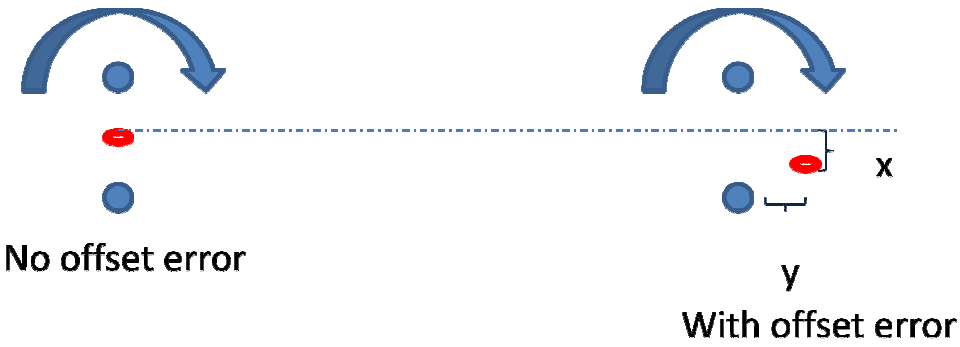

Figure 4.19 DUT offset on Turn table

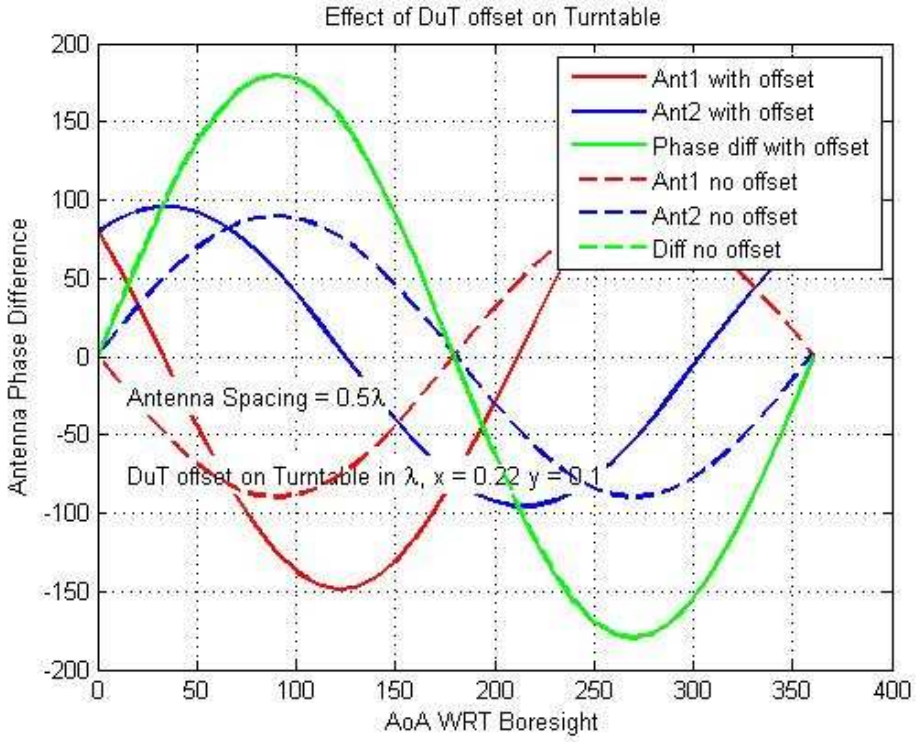

Figure 4.20 Effect of DUT offset on Turntable, a prediction

Different values for x and y offsets were tried to get the close match on the ideal phase difference between two antenna elements. The phase response shown in figure 4.7 is taken as reference and as it can be seen in that figure, one element has a swing of about 200 degrees and the other element has total swing of about 300 degrees. The values x=0.22 and y=0.1 (in terms of lambda) gives a very tight match on the reference phase response. This is shown in figure 4.20. The solid red and solid blue line gives the desired swing for each element with this offset. The dashed lines show the ideal response. The comparison between the ideal phase response and the phase response with for DUT offset is shown in figure 4.21. The correction phase for each AoA is plotted in figure 4.22. Using this phase the prediction for the measured correlation is calculated again.

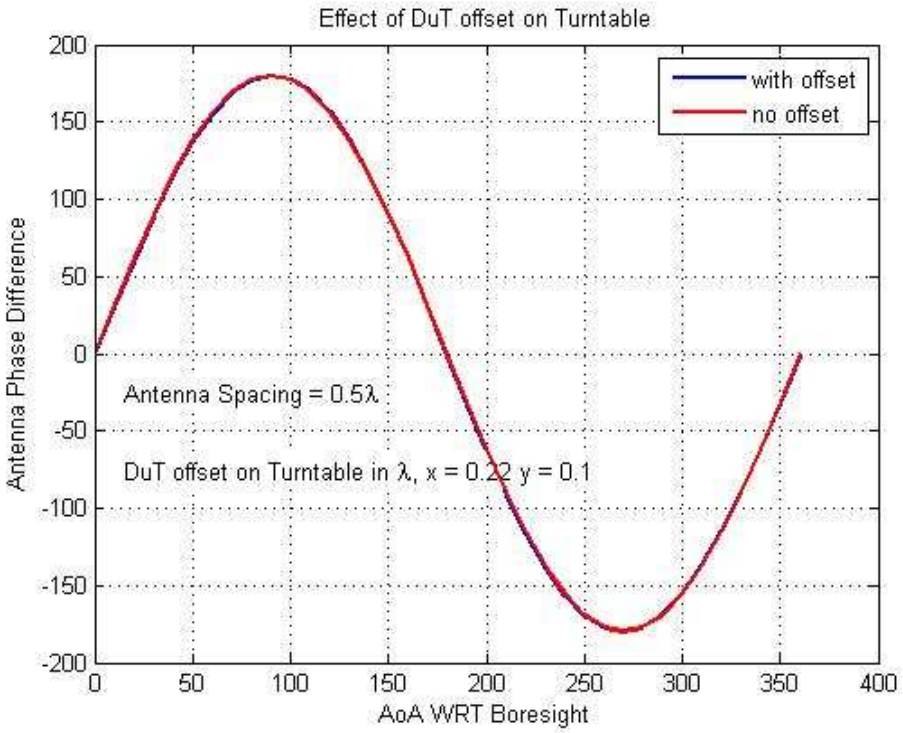

Figure 4.21 Antenna Phase Difference comparison for DUT offset on Turntable

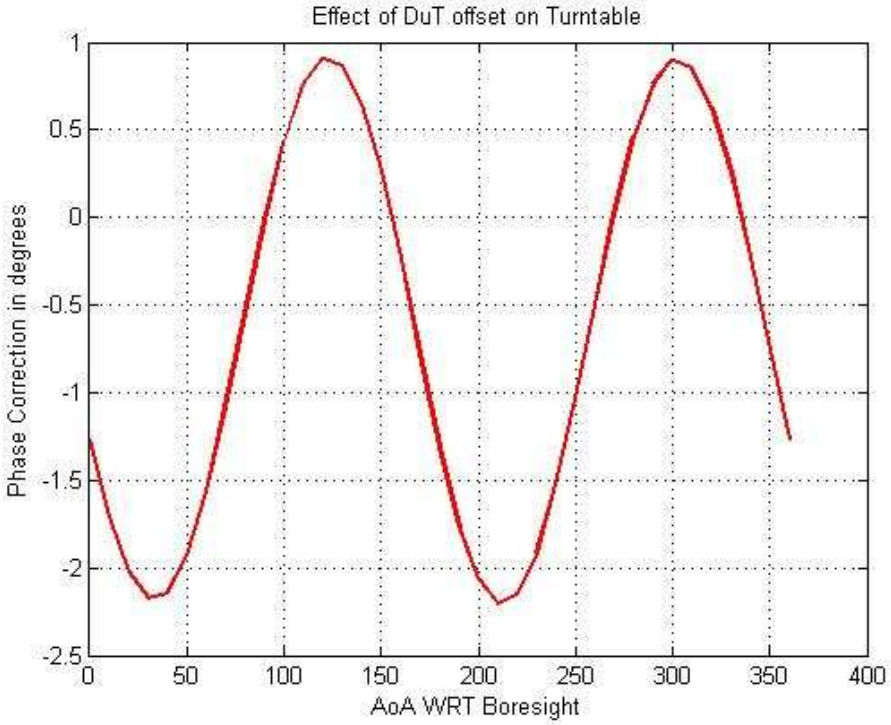

Figure 4.22 Phase correction for the DUT offset on Turntable

Although, the corrected phase is used to predict the correlation coefficient values it is observed that this correction is not sufficient to improve the match drastically. It is recommended to use very high precise probe elements at receiver which will have good decoupling capabilities to combat this issue.

CHAPTER 5

SUMMARY AND CONCLUSIONS

5.1 Summary

A spatial correlation measurement system was developed to test the OTA performance of the MIMO channel link inside an anechoic chamber. The necessary qualitative analysis was carried out to justify that the 3 component model will represent a real world narrow angel spread signal model characterizing a cluster of multipath frequency selective fading environment observed in 1900 MHz wideband cellular channel.

The automated measurement test set is developed using the Lab VIEW programming VI's and the measuring instruments were integrated to take concurrent measurements of the received signal. Different sets of antenna elements were used for the spatial correlation measurements.

System repeatability is tested by taking 3 different data sets for antenna pattern measurements. The actual measurements for spatial correlation coefficients are carried out with two different sets of the antenna elements. The analysis of the measured data with respect to the predicted values is carried out and the limitations of the measurement set up were investigated.

5.2 Conclusions

I. The *first-order* statistics of the measured data confirmed that the real world Rayleigh fading channel was created inside the chamber to carry out the OTA testing for the MIMO link. It is important to know that the MIMO channel model used for the OTA testing should represent the real world multipath narrow angle spread signals. The CDF for the

received signal using 3 component model matches exactly with the ideal curve for the fade depths up to 40dB.

II. The measured data confirms that the spatial channels can be created inside the anechoic chamber and the spatial correlation can be used to compare the channel statistics. This is the first step towards determining the figure of merit for MIMO OTA testing. In order to carry out throughput measurements for MIMO channels using OTA techniques it is necessary to distinguish between the good and bad MIMO terminals. The spatial correlation measurements can be used to examine the OTA testing signal. This technique uses spatial correlation to analyze the ability to reproduce the spatial sequences for OTA testing.

III. The spatial correlation measurements technique allows us to distinguish between the MIMO propagation effects and the antenna effects. This has imperative merit while evaluating the MIMO OTA test signal used in throughput measurements.

IV. For the prediction of the spatial correlation coefficients the antenna voltage gains were normalized in two different ways. In first approach the voltage gains were normalized to unit voltage and in the other approach the magnitudes were normalized to the unity power. It is observed that the spatial correlation by default normalizes the gain values so the normalization method will not affect the final answer. The two prediction curves were almost touching to each other. In this work the normalization to unity power approach is used for the analysis of the spatial correlation measurements.

V. While analyzing the prediction curves with respect to the measured data for the spatial correlation measurements it is observed that the measurements are more sensitive to the phase relations than the gain relations. For real gain case, if you use the real phase and the ideal phase, then you can clearly see that the correlation envelope is changed a lot. But on the contrary, if you keep the phase relation constant and then changed the gain to predict the values, then you can see that the envelope shape is maintained and only a magnitude change is observed.

VI. Although the spatial correlation measurements are more sensitive to phase relations, the effect of decoupling at the antenna element is equally important. The measurements are sensitive to both gain and phase relations but more over the repeatability can be obtained only by achieving good decoupling at the antenna elements. Lab precision dipoles which are highly tuned to the operating frequency should be used to achieve a good match between the predicted and measured data.

VII. The correlation comes from the phase difference at the MS and the azimuthal angle spread observed in spatial channel models. Thus it becomes necessary to model the angle spread carefully. It is confirmed that the 3-copmonent prefaded model emulates the angle spread observed in the spatial channel model.

VIII. The spatial correlation measurements can be linked to the complex path gains of the channel matrix and using those gains the channel capacity can be estimated. The correlation is inversely proportional to the channel capacity. High correlation values represent the weaker multipath or scattering environment and this in turn reflects the lower channel capacity. On the other hand lower correlation coefficients represent the rich scattering environment and which in turn reflects the higher channel capacity.

IX. The VNA used in the set-up could sample the data at a maximum rate of 17 samples per second. This is crucial in determining the measurement time. This is because in order to get good fading statistics for the time evolved spatial sequences, enough number of samples needs to be collected. This limitation acts as an upper bound on the maximum Doppler shift that can be used at the fader boxes which reflects the velocity of the mobile terminal.

X. The system repeatability was checked to evaluate its performance reproducibility. Three sets of antenna pattern measurements were carried out and there statistical comparison is shown in table 5.1.

Table 5.1 Repeatability statistics of the Antenna pattern measurements

Set	Expected value of Gain Magnitude for antenna 1 (Normalized Voltage gains)	Expected value of Gain Magnitude for antenna 2 (Normalized Voltage gains)	Expected value of Phase Magnitude for antenna 1 (in Radians)	Expected value of Phase Magnitude for antenna 2 (in Radians)
1	0.7546	0.7720	1.0481	0.2407
2	0.7450	0.7651	1.0614	0.2292
3	0.7609	0.7750	1.0488	0.0652

Set-1 values were used throughout the work to estimate the expected correlation values. With set-1 as reference, the gain and phase on each antenna elements differ not more than 2% of the original value.

XI. The comparison between the measured and predicted values for the complex envelope correlation coefficients is given in table 5.2.

Table 5.2 Comparison between measured and predicted values for the spatial correlation coefficients

	Sleeve Dipoles (omni coupled)	Precision Dipoles Set 1 (Omni coupled)	Precision Dipoles Set 1 (Omni coupled) Drooping Power	Precision Dipoles Set 2 (Omni coupled)	Precision Dipoles Set 2 (Omni un coupled)
Real Gain Real Phase	-	0.4458 (+3.43%)	0.3333 (-22.73%)	0.446 (+2.599%)	0.4462 (+2.645%)
Real Gain Ideal Phase	-	0.4199 (-2.57%)	0.316 (-26.682%)	0.4202 (-3.33%)	0.3383 (-22.17%)
Ideal Gain Ideal Phase	0.5271 (-5.65%)	0.5626 (+30.53%)	0.4581 (+6.28%)	0.5637 (+29.67%)	0.3623 (-16.65%)
Ideal Gain Real Phase	-	0.5942 (+37.86%)	0.4811 (+11.624)	0.5951 (+36.89%)	0.5082 (+16.90%)
Measured	0.5587	0.431	0.431	0.4347	0.4347

When the antenna pattern gain and phase values are used to predict the complex envelope correlation coefficients, the prediction value gives a good match to the measured values.

5.3 Future Work

The background technical work for the standardization of the over-the-air (OTA) testing of MIMO terminals is on-going. This work can be extended to test the full terminal performance of a wideband multipath frequency selective MIMO channel. In this work a cluster of narrow angle spread signals was simulated and tested in the chamber. In order to perform the OTA testing of the multi cluster modes of the MIMO channel it is necessary to move form 3-Component model to multi component model. However it should be remembered that the main objective of the MIMO channel modeling is to reduce the number of transmitters required to reproduce the real world fading scenario.

The possibilities of such a MIMO OTA measurement system where *K* number of OTA antennas are located on the entire 360 º azimuth angle region with 360 º/K intervals and these OTA antennas can be used to synthesize a desired plane wave field in the test zone located in the center of the OTA antenna circle.

Analyzing the effect of polarization dispersion is on more challenging area in MIMO OTA testing.

APPENDIX A

TECHNICAL SPECIFICATIONS FOR THE RF CHANNEL EMULATOR UNITS PROVIDED BY SPIRENT COMMUNICATIONS

The following specifications describe warranted performance over the temperature range 0 – 40° C and include a 30-minute warm-up tim e from ambient conditions. These specifications are obtained directly from the product datasheet supplied by the Spirent Communications.

RF Inputs: 2 (inter-unit synchronization allows up to 8)

RF Outputs: 2 (inter-unit synchronization allows up to 8)

Digital Channels: 2 per unit (4 with MIMO Option, future expansion to 8)

RF Configurations: SISO, SIMO, MISO, MIMO (2x2, 2x4, 4x2, 4x4), and Beamforming

Bandwidth: 26 MHz

RF Input Frequency Range: 400 – 2700 MHz

(w/ 6-GHz-EX option):3300 – 3850 MHz, 4100 – 6000 MHz

Level Range +5 to -32 dBm @ 400 to 2700 MHz

(w/ 6-GHz-EX option): -5 to -32 dBm @ 3300 to 3850 MHz

(w/ 6-GHz-EX option):-5 to -32 dBm @ 4100 to 6000 MHz

Level Resolution: 0.1 dB

Damage Level > +20 dBm

RF Output Level Range:-30 to -110 dBm @ 400 to 2700 MHz

(w/ 6-GHz-EX option): -35 to -110 dBm @ 3300 to 3850 MHz

(w/ 6-GHz-EX option):-40 to -80 dBm @ 4100 to 6000 MHz

Resolution: 0.1 dB

Accuracy: ± 1 dB

Residual EVM Better than -36 dB, typical per subcarrier measured at -50 dB output power;

Actual value depends upon signal format, symbol rate, etc.

RF Port VSWR: Better than 1.5:1.

Independent Paths: 24 (24 paths per channel w/ MIMO option)

Relative Path Delay: 0 – 2000 μs, 0.1 ns resolution.

Relative Path Loss: 0 – 32 dB

Fading:

Types: Rayleigh, Rician, freq shift, phase shift

Fading Velocity: 0.1 to 2398.33 km/h @ 900 MHz; Resolution of 0.1 km/h

Repetition Interval: > 24 hours

Relative Phase: 0 – 360 degrees, 0.1 degree resolution

Rician K factor: -30 to +30 dB

Level Crossing Rate (LCR) Accuracy: < ± 2.5% deviation from theoretical LCR curve of the simulated vehicle velocity

Fading Power Spectrum: Classical 6 dB, Flat, Classical 3 dB, Rounded, Rounded 12 dB

Correlation: Envelope and Component; Complex correlation is included with MIMO option

Log-Normal Fading:

Fading Rate: 0.00 to 20.00 Hz

Standard Deviation: 0 to 12 dB

MIMO Option Modes Baseline: 2x2 Modularity expandable to uni/bi-directional 2x4, 4x2, 4x4

AWGN Option:

C/N Ratio -30 to +32 dB

Accuracy: ±0.1 dB for -20 to 15 dB ratios

Bandwidth: 26, 13, 6.5, 3.25, 1.625 MHz. Fidelity Meets or exceeds all 3GPP, 3GPP2, WLAN, WiMAX, and LTE requirements.

Sequence Duration: > 2 hours

Settable Modes: C/N, C/No, Eb/No

REFERENCES

[1] "Increasing capacity in wireless broadcast systems using distributed transmission/directional reception," by A. J. Paulraj and T. Kailath, US Patent, no. 5,345,599, 1994.

[2] “Layered Space-Time Architecture for Wireless Communication in a Fading Environment When Using Multi Element Antennas”, by Gerard J. Foschini, Bell Labs Tech. Journal, Autumn 1996, pp 41-59.

[3] "Spatio-temporal coding for wireless communication," by G. G. Raleigh and J. M. Cioffi, IEEE Trans. Communications, vol. 46, no. 3, pp. 357-366, 1998.

[4] “On Limits of Wireless Communications in a Fading Environment when Using Multiple Antennas,” G. J. Foschini and M. J. Gans, Wireless Personal Communications, no. 6, pp. 315–335, 1998.

[5] “A Discrete-Time Model for Triply Selective MIMO Rayleigh Fading Channels”, by Chengshan Xiao, Jingxian Wu, Sang-Yick Leong, Yahong Rosa Zheng and Khaled Ben Lataief, IEEE Trans. on Wireless Communications ,Vol. 3 No.5 ,September 2004

[6] “Spatial Correlation and Capacity Measurements for Wideband MIMO Channels in Indoor Office Environment”, by Padam L. Kafle , Apichart Intarapanich ,Abu B. Seasy, John McRory and Robert J.Davies, IEEE Trans. on Wireless Communications ,Vol. 7 No.5 ,May 2008

[7] “The Use of Ray Tracing Models to Predict MIMO Performance in Urban Environments”, by Carmen Cerasoli, pp.1-8, MILCOM 2006,

[8] “New Wireless Technologies and OTA Measurements”, by Dr.Chrostoph Von Gagern, Antenna and Propagation 2007 Eu-CAP 2007.

[9] “ An Interim Channel Model for Beyond -3G Systems, Extending the 3 GPP Spatial Channel Model (SCM) “, by D.S. Baum, J. Salo, G. Del Galdo, M. Milojevic, P. Kyösti, and J. Hansen, in Proc. IEEE Vehicular Technology Conference 2005 Spring, Stockholm, May 2005.

[10] “Classifications of MIMO Channel Models”, by Rashmi Verma, Shilpa Mahajan and Vishal Rohila, Networks, 2008. ICON 2008. 16th IEEE International Conference on**.**

[11] “Antenna Spacing Effects on Indoor MIMO Channel Capacity”, by Jiangang Lv Yinghua Lu Yeqiu Wang Hongtao Zhao Chun Yuan Han,Microwave Conference Proceedings, 2005. APMC 2005. Asia-Pacific Conference Proceedings

[12] “On The Number of OTA Antenna Elements for Plane-Wave Synthesis in a MIMO OTA Test System Involving Circular Antenna Array”, by T.Laitinen, P. Kyösti, J.-p. Nuutinen , Pertti Vainikainen,COST 2100 TD(09)976,September 2009.

[13] “Spatial channel model for Multiple Input Multiple Output (MIMO) Simulations “ (Release 7),3GPP TR 25.996 V7.0.0(2007-06)

[14] “Spatial channel model for Multiple Input Multiple Output (MIMO) simulations”, 3GPP TR 25.996, version 6.1.0, September, 2003.

[15] “Requirements for MIMO OTA test equipment”, Elektrobit, Spirent Communications, ETS-Lindgren, LG Electronics, Nokia, Motorola, (*), 3GPP RAN4 contribution R4 092941, Shenzhen, China, Aug. 24- 28, 2009.

[16] “Channel Models for MIMO OTA”, Elektrobit, Spirent Communications, 3GPP RAN4 contribution R4-092943 Shenzhen, China, Aug. 24- 28, 2009.

[17] “MIMO OTA test methodology proposal”, R4-091361, Agilent Technologies.

[18] “Practical MIMO OTA Testing”, R4-091362, Spirent Communications.

[19] “OTA for MIMO”, 3GPP R4-091763, Spirent Communications.

[20] “Experiments in Spatial Correlation”, COST2100, TD (09)856, Spirent Communication.

[21] “Practical Aspects of MIMO OTA Testing”, (Spirent) 3GPP R4-092320.

[22] “Practical Considerations on MIMO OTA testing”, COST2100, TD (09)854, Satimo, Electrobit, May 2009.

[23] “Anechoic Chamber Reflections in OTA Measurements “, COST2100, TD (09)9102, Spirent Communications.

[24] “Fundamental tradeoffs in MIMO wireless systems”, by H. Boelcskei, IEEE 6th CAS Symp. on Emerging Technologies: Mobile and Wireless Comm. Shanghai, China, May 31-lune 2,2004

[25] “Introduction to Space- Time Wireless Communications”, by Arogyaswami Paulraj, Rohit Nabar, Dhananjay Gore, and Cambridge press, 2003.

[26] “Antenna Theory Analysis and Design”, 2nd Edition by Constantine A. Balanis ,2007

[27] “Probability and Random Processes for Electrical Engineering”, 2nd Edition by Leon Garcia, 1994.

[28] “Wireless Communications Principle and Practice”,2nd Edition by Theodore S. Rappaport ,2006

[29] “MIMO Efficiency of a LTE Terminal Considering Realistic Antenna Models” , by Alexander Geibler, Volker Wienstroer,Rainer Kronberger , Frank Dietrich , Christian Drewes, International ITG workshop on Smart Antennas-WSA 2009

[30] www.wikipedia.org

[31] “Correlation-Based Spatial Channel Modeling”, White Paper 100, Spirent Communications, 2008.

BIOGRAPHICAL INFORMATION

Digvijay Arjunrao Jadhav was born on 3rd June 1984 in Pune, Maharashtra, India. He did his Bachelor of Engineering in the field of Electronics and Telecommunications Engineering from the Maharashtra Institute of Technology, University of Pune, India in June 2005. Later then, he worked as a RF Engineer in an Indian telecommunications giant, Reliance Communications (formerly known as Reliance Infocomm) in Pune, India. After working in the industry for a while he decided to pursue his Master's. In spring 2007 he joined the graduate program in Electrical Engineering at The University of Texas at Arlington, Texas, USA. In fall 2007 he joined the Wave Scattering Research Center (WSRC) at UTA and started working under the guidance of Dr. Jonathan Bredow. Since then he has worked as GTA and GRA for the Department of Electrical Engineering at UTA. While working at WSRC, along with the research work, he carried out the RF testing for several industrial projects. He is a member of the honors society, Etta-Kappa-Nu (HKN) since November 2007. He adores RF and he is more like a hands-on guy who believes in learning the principles of the RF Testing and Engineering by actually performing the measurements which simulates the real world situations. His current research interests include working in the field of RF and Microwave Engineering and finding new OTA testing techniques for RF and Wireless Systems.